

Hardware-Efficient Entanglement Distillation Using Bosonic Systems

Shoham Jacoby,^{1,2} Rotem Arnon-Friedman,³ and Serge Rosenblum¹

¹*Department of Condensed Matter Physics, Weizmann Institute of Science, Rehovot, Israel*

²*Racah Institute of Physics, The Hebrew University of Jerusalem, Jerusalem 91904, Givat Ram, Israel*

³*Department of Complex Systems, Weizmann Institute of Science, Rehovot, Israel*

(Dated: March 14, 2025)

High-fidelity entanglement shared between distant quantum systems is an essential resource for quantum communication and computation. Entanglement distillation addresses this need by converting multiple noisy Bell pairs into fewer higher-fidelity pairs, using only local quantum operations and classical communication. However, this approach typically requires a substantial overhead in the number of qubits. To bypass this hurdle, we propose to leverage the high-dimensional Hilbert space of a *single* pair of bosonic systems to store a large amount of entanglement, replacing the need for multi-qubit systems. To distill entanglement in such a setup, we devise a new entanglement distillation protocol, tailored for bosonic systems. The protocol converts a highly-entangled noisy state between two bosonic systems into a lower-dimensional but high-fidelity entangled state, using only local bosonic operations. We show that our protocol significantly enhances the fidelity of the entangled state in the presence of naturally occurring loss and dephasing errors. Compared to methods relying on multiple Bell pairs, our scheme offers a more hardware-efficient strategy, providing a practical route toward the realization of entanglement distillation.

I. INTRODUCTION

Entanglement between spatially separated quantum systems plays a crucial role in quantum communication [1–3], quantum cryptography [4, 5], and distributed quantum computing [6, 7]. However, establishing and maintaining high-fidelity entanglement between distant parties remains a significant challenge due to inherent noise in the preparation and distribution process that degrades the entangled states.

Entanglement distillation, also known as entanglement purification, offers a promising solution [8–12].

Typically, distillation protocols process multiple noisy entangled qubit pairs to extract a smaller number of higher-fidelity pairs [8–10] using only local operations and classical communication (LOCC) — the operations available to the two distant parties, each acting on their own local systems. Although entanglement distillation has been demonstrated experimentally [13, 14], these experiments have been limited to distilling only one high-fidelity pair from two noisy ones. Achieving a Bell-pair fidelity high enough for useful applications requires a large number of initial qubits and operations [15, 16], which poses significant technological challenges and introduces potential points of failure that can further degrade the fidelity.

To address similar hardware overhead challenges in quantum error correction, bosonic systems have been used as an alternative to two-level systems [17]. The high-dimensional Hilbert space of bosonic systems enables redundant encoding of logical qubits, leading to more hardware-efficient error correction protocols [17–21]. Bosonic quantum error correction has been realized experimentally for a variety of encodings, such as GKP [17, 22] and Schrödinger cat codes [23, 24]. The hardware-efficiency of this method has enabled bosonic systems to exceed the break-even point of quantum error correction

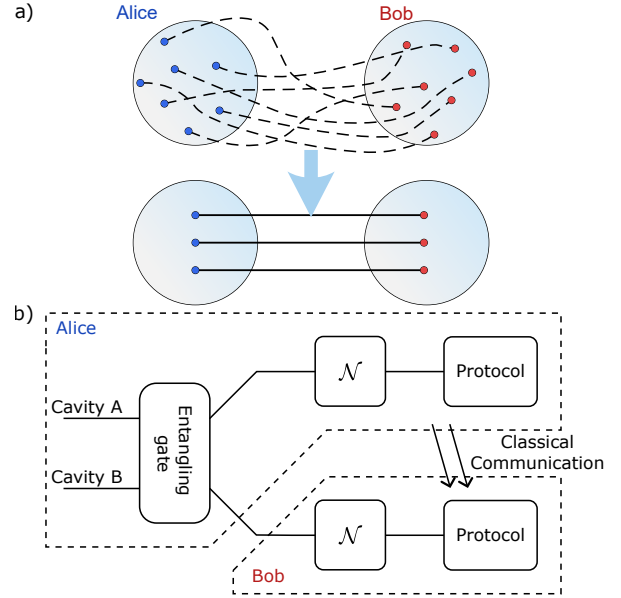


FIG. 1. **(a)** Top: Schematic representation of a highly entangled initial state between two cavities with low fidelity (represented by dashed lines). Bottom: The entanglement distillation protocol enhances the state fidelity, but reduces the total entanglement (solid lines). **(b)** The distillation protocol begins with Alice performing an entangling gate and sending one of the cavities to Bob. The cavities are subject to a loss-dephasing channel \mathcal{N} . Alice and Bob then recover a high-fidelity entangled state using local operations and classical communication.

[25–29].

In this work, we propose to use bosonic systems for achieving hardware-efficient entanglement distillation. The high degree of entanglement between the bosonic systems is achieved by populating multiple energy levels of the high-dimensional bosonic Hilbert space. We devise

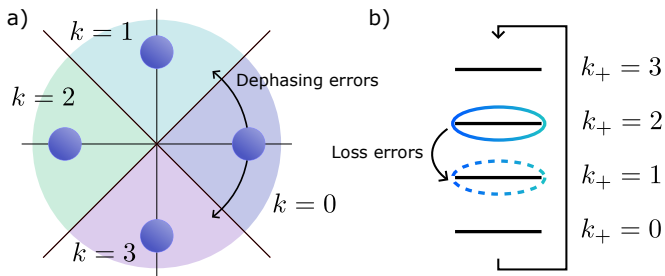


FIG. 2. **(a)** Each qudit is encoded in a bosonic system by dividing its phase space into d angular sections. In this computational basis, dephasing errors correspond to the application of cyclic raising or lowering operators. **(b)** The dual qubit basis corresponds to a modular photon-number representation, with photon loss acting as a cyclic lowering operator.

a novel protocol that performs entanglement distillation using only a *single* pair of bosonic systems, rather than relying on multiple copies of entangled two-qubit systems. Similar to qubit-based schemes, the initial state used in our protocol is in principle straightforward and natural to produce in experimental settings. Our distillation protocol then acts on the noisy initial state and produces a final state with enhanced fidelity while reducing the total effective size of the Hilbert space. This setup is illustrated in Fig. 1a.

Our proposed distillation protocol is markedly different from traditional multi-qubit entanglement distillation. While it is true that a bosonic system can be thought of as a tensor product of multiple two-level systems, the native errors and gates on the bosonic system do not respect this tensor-product structure. Thus, standard entanglement distillation protocols used for qubits are not appropriate. Instead, a more adequate approach is to treat the cavities as qudits encoded in a basis that is natural to bosonic systems. In particular, we use discrete rotation symmetry in cavity phase space to define the encoding, inspired by the bosonic rotation codes introduced by Grimsmo et al. [21]. This choice is motivated by the effectiveness of these quantum error-correcting codes against naturally occurring loss and dephasing noise. Since our method uses non-Gaussian operations, previous no-go results on distillation from multiple pairs of entangled bosonic systems using Gaussian operations do not apply [30, 31]. We show both analytically and numerically that our method enables entanglement distillation with high performance while minimizing the amount of necessary hardware.

The rest of the paper is arranged as follows. In Section II, we show how to model noisy entanglement in bosonic systems and present our bosonic entanglement distillation protocol. We analyze the protocol’s performance both analytically and numerically. Then, in Section III, we propose a procedure to implement our protocol in a two-cavity system, where two initially non-entangled cavities are prepared in a squeezed coherent state and manipulated using controlled rotation gates [21].

II. BOSONIC ENTANGLEMENT DISTILLATION

As illustrated in Fig. 1b, the distillation process begins with one party, Alice, preparing a state with high entanglement entropy E_i [9] in two bosonic systems, henceforth referred to as cavities A and B .

Following this state preparation, Alice transmits cavity B to Bob. During transmission, both cavities are subject to photon loss and dephasing, which are common noise channels in bosonic systems [32]. Photon gain errors occur at a significantly lower rate in typical experimental settings and are therefore not considered in this study. Nevertheless, our protocol can be straightforwardly extended to incorporate these errors as well. The loss-dephasing noise channel reduces the fidelity of the two-cavity state to the ideal entangled state.

To restore a high-fidelity state, Alice and Bob apply an entanglement distillation protocol. The general form of the protocol is as follows: first, each party conducts specific measurements on their respective cavities. Alice then communicates her measurement outcomes to Bob. Based on these outcomes, both parties apply bosonic operations on their cavities. The end result of this protocol is a distilled state that has higher fidelity to a desired target state, albeit with reduced entanglement entropy E_f . In the next sections, we elaborate on each stage of the distillation procedure.

A. Encoding highly entangled bosonic states

We define the bosonic qudit by dividing the cavity phase space into d angular sections, and associating the qudit state $|k\rangle$ with the k^{th} angular interval $\frac{(2k-1)\pi}{d} \leq \phi < \frac{(2k+1)\pi}{d}$ (Figure 2a). A definition using continuous variables is provided in Section III A. For simplicity, we choose d to be a power of two, i.e., $\log d \in \mathbb{N}$.

We can now introduce our highly entangled initial state

$$|\psi_i\rangle = \frac{1}{\sqrt{m_i}} \sum_{k=0}^{m_i-1} \left| \frac{d}{m_i} k \right\rangle_A \otimes \left| \frac{d}{m_i} k \right\rangle_B, \quad (1)$$

where m_i is the initial number of “legs”, i.e. the number of basis states participating in the superposition. We show in Section III A that this initial state is convenient to prepare in bosonic systems. The entanglement entropy between the cavities at the onset of the distillation protocol is thus $E_i \equiv H(\text{Tr}_A |\psi_i\rangle \langle \psi_i|) = \log m_i$, where $H(\rho) \equiv -\text{Tr}(\rho \log \rho)$ is the von Neumann entropy of a state ρ , and Tr_A denotes the partial trace over subsystem A . For simplicity, we assume $m_i = d$ unless stated otherwise.

B. Discretized error model

While transferring cavity B from Alice to Bob, both cavities are affected by dephasing and photon loss channels

Protocol 1 Bosonic entanglement distillation

Arguments:

- m_i – The dimension of the single-cavity subspace supporting the initial state, corresponding to the angular phase-space symmetry of the initial state.
 - m_c – The dimension of the single-cavity subspace supporting the intermediate qudit obtained after the first measurement stage.
 - m_f – The dimension of the single-cavity subspace supporting the final qudit obtained after both measurement stages.
 - $f_{\text{cut}} \in \{0\} \cup [1/m_f^2, 1)$ – The cut-off fidelity below which the protocol is aborted.
 - all dimensional arguments are restricted to powers of two ($\log m_x \in \mathbb{N}$) and follow the relation: $2|m_f|m_c|m_i|d$, where $|$ stands for “divides”.
- 1: **Both parties** perform modular $\Delta_c \equiv \frac{d}{m_c}$ measurements in their qudit’s computational basis and register their results as A_1 and B_1 , respectively.
 - 2: **Alice** sends her result to Bob and **Bob** determines u_B according to a pre-calculated dictionary based on both results (Eq. (B14)).
 - 3: **Alice and Bob** rotate their states by X^{-A_1} and $X^{-B_1+u_B\Delta_c}$, respectively.
 - 4: **Both parties** perform modular $\Delta_f \equiv \frac{m_c}{m_f}$ measurements in their qudits’ dual basis and register their results as A_2 and B_2 , respectively.
 - 5: **Alice** sends her result to **Bob** who uses a second pre-calculated dictionary to determine v_B (Eq. (B21)).
 - 6: **Alice and Bob** rotate their states in the dual basis, applying Z^{-A_2} and $Z^{-B_2-v_B\Delta_f}$, respectively.
 - 7: **Abort** if the calculated expected fidelity $\mathcal{F}(A_1, B_1, A_2, B_2) \leq f_{\text{cut}}$ (Eq. (B25) in the Appendix).
-

(see Appendix A 1). Because these channels commute [32], we can assume they act consecutively on the input state. The dephasing channel results in a rotation of the cavity phase space, leading to cyclic shift errors in the computational (angular) basis (see Figure 2a). The resulting discretized dephasing errors D_s , which shift the state by s angular sections, are equivalent to the generalized Pauli operators [17] X^s , with $-d/2 < s \leq d/2$, i.e.:

$$D_s \equiv X^s : |k\rangle \rightarrow |k + s \pmod{d}\rangle . \quad (2)$$

The corresponding dephasing error probabilities $\{p_s^D\}$, which decay super-exponentially with $|s|$, can be derived using the rate of the bosonic dephasing channel, γ_ϕ (see Appendix A 2).

The loss channel is more conveniently expressed in the dual modular photon-number basis (Figure 2b), whose basis states $|k_+\rangle$ are Fourier transforms of the d computational states

$$|k_+\rangle \equiv \frac{1}{\sqrt{d}} \sum_{j=0}^{d-1} e^{-2ijk\pi/d} |j\rangle . \quad (3)$$

In this basis, the loss of l photons can be approximately modeled by a cyclic shift, which is equivalent to the generalized Pauli operator Z^{-l} , where $l \geq 0$:

$$L_l \equiv Z^{-l} : |k_+\rangle \rightarrow |(k-l)_+ \pmod{d}\rangle . \quad (4)$$

The corresponding error probabilities $\{p_l^L\}$ can be approximated using the average photon number \bar{n} and the rate γ_l associated with the bosonic loss channel (Appendix A 2). These probabilities also decrease super-exponentially with l . Henceforth, the modulo symbol will be omitted for brevity.

This discretized qudit error model, while not exact, is a reasonable approximation for our purposes, as we show numerically in Section III B. For two cavities undergoing both loss and dephasing noise, we define the set of possible errors, \mathcal{E} , and calculate the corresponding probability $p(\bar{x}) = p_{s_A}^D p_{s_B}^D p_{l_A}^L p_{l_B}^L$ of each error $\bar{x} = (s_A, s_B, l_A, l_B) \in \mathcal{E}$. Applying this noise channel to the initial state from Equation (1), and considering all possible errors, we obtain the density matrix

$$\rho = \sum_{\bar{x} \in \mathcal{E}} p(\bar{x}) |\varphi_{\bar{x}}\rangle \langle \varphi_{\bar{x}}| , \quad (5)$$

where $|\varphi_{\bar{x}}\rangle$ is the error state associated with \bar{x} :

$$\begin{aligned} |\varphi_{\bar{x}}\rangle &= L_{l_A}^A L_{l_B}^B D_{s_A}^A D_{s_B}^B |\psi_i\rangle \\ &= L_{l_A}^A L_{l_B}^B \sum_{k=0}^{m_i-1} |k\rangle_A |k + \delta_s\rangle_B , \end{aligned} \quad (6)$$

with $\delta_s = s_B - s_A$.

C. Entanglement distillation protocol

After both cavities undergo the loss-dephasing channel, Alice and Bob apply the distillation protocol using LOCC operations to achieve a high-fidelity entangled state (see Protocol 1). In the following sections, we present the protocol in a general setting, followed by an example with a four-level qudit encoding.

In the first of three stages of the protocol (Fig. 3c-d), Alice and Bob measure their cavities with modular phase measurements to address dephasing errors. In the second stage (Fig. 3g-h), they perform modular measurements

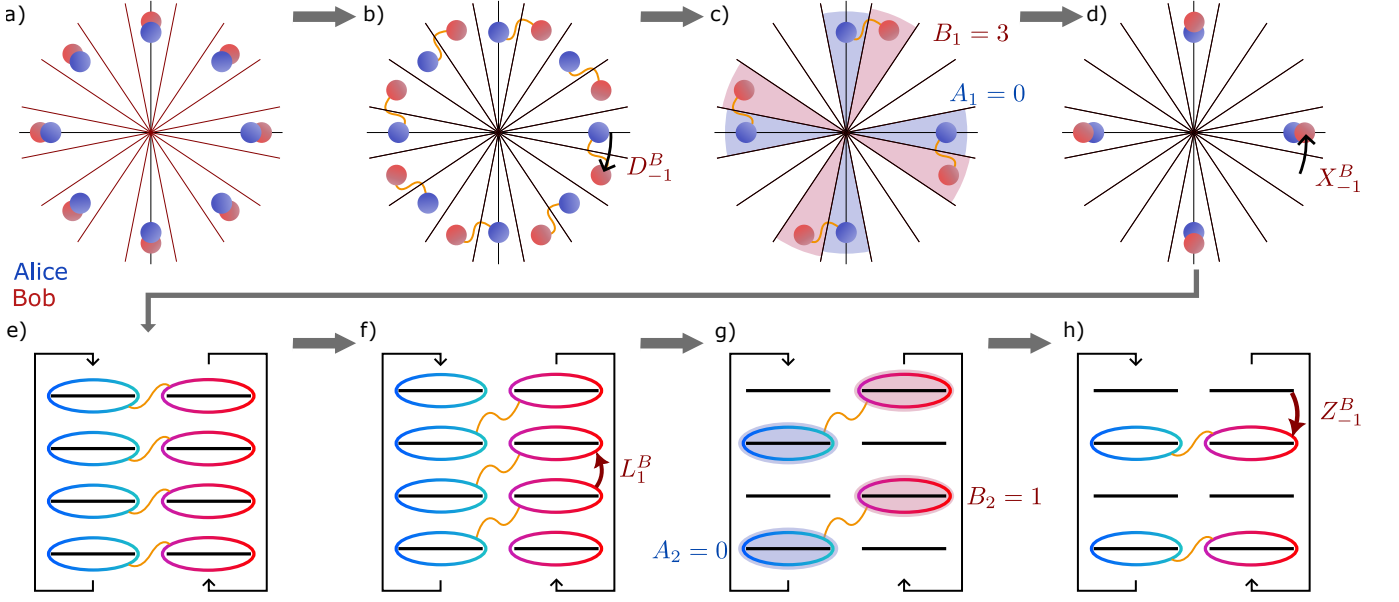


FIG. 3. Schematic representation of the entanglement distillation protocol with $d = 16$, $m_i = 8$, $m_c = 4$, and $m_f = 2$. Alice's and Bob's phase space distributions are illustrated in blue and red, respectively. Here, we choose $m_i \neq d$ for improved clarity. (a) The protocol starts with the two cavities in the initial entangled state. (b) The cavities then undergo dephasing noise. In this example, only Bob's cavity is affected by D_{-1}^B . (c) Next, both parties carry out a modular phase measurement with $m_c = 4$, which projects the state onto a four-dimensional subspace for each cavity. (d) Next, the parties share their measurement outcomes. In this example, only Bob rotates his cavity phase space to realign with that of Alice. The second stage of the protocol, which addresses photon loss, is illustrated in (e-h). Alice's and Bob's cavities are depicted in the modular photon-number basis on the left and right sides, respectively. Due to the negative sign in Bob's cavity (see Eq. (9)), photon loss results in shifts in opposite directions, as indicated by the arrows representing photon-number modularity. Similarly to the top panel, the bottom panel represents (e), the initial noiseless cavities, (f), the cavities after undergoing the photon loss channel, (g), the modular photon-number measurements, and (h), realignment by the parties after communicating the measurement outcomes.

in the dual number basis to address photon loss errors. Finally, in a third stage, the parties decide whether or not to abort the protocol, based on the measurement outcomes.

Modular phase measurements – The modular phase measurement is represented by the set of projection-valued measurement elements (PVMs), $\{P_x^{\Delta_c}\}_{x=0}^{x=\Delta_c-1}$, where x is the measurement outcome corresponding to the angular section modulo Δ_c , with Δ_c a power of two between 1 and m_i . Each PVM element can be written as

$$P_x^{\Delta_c} = \sum_{j=0}^{d/\Delta_c-1} |j\Delta_c + x\rangle \langle j\Delta_c + x|. \quad (7)$$

This measurement restricts the qudit from the initial subspace of dimension m_i to a subspace of dimension $m_c \equiv d/\Delta_c$ (see Fig. 3c). m_c is a key parameter of the protocol. A lower m_c will result in higher robustness against dephasing errors, while a higher m_c will result in higher robustness against loss errors; a detailed discussion of this trade-off will be presented in Section II E. We note that increasing m_i while keeping m_c fixed does not enhance protection against dephasing errors (Appendix E). However, as we show in Section III A, choosing a higher m_i can lead to improved state preparation fidelity.

Alice and Bob each apply a modular phase measurements to their respective cavity, yielding outcomes A_1 and B_1 . These measurements project the m_i -legged state to an m_c -legged state (with $m_c \leq m_i$) rotated by A_1 (B_1) sections relative to the state $|0\rangle_{A(B)}$. Due to the dephasing noise, the measurement outcomes A_1 and B_1 will differ by $\delta_s \bmod \Delta_c$. Using Eqs. (6) and (7), we obtain the post-measurement state

$$|\tilde{\varphi}_{\tilde{x}}\rangle = \frac{1}{\sqrt{m_c}} \sum_{k'=0}^{m_c-1} c_{k'} |\Delta_c k' + A_1\rangle_A |\Delta_c(k' + u) + B_1\rangle_B, \quad (8)$$

with $u = \frac{\delta_s + A_1 - B_1}{\Delta_c}$ an integer. $|c_{k'}| = 1$ accounts for loss errors and can be ignored for the examination of the first stage of the protocol (see Appendix B).

This expression highlights two types of misalignment between the cavities: one where each cavity is rotated with respect to the state $|0\rangle_{A(B)}$ by A_1 (B_1), and another where the cavities are rotated by $u\Delta_c$ with respect to each other. Both parties need to rotate their cavities to address those misalignments, with the objective of achieving the intermediate target state $\frac{1}{\sqrt{m_c}} \sum_{k'} c_{k'} |\Delta_c k'\rangle_A |\Delta_c k'\rangle_B$.

To align her cavity with $|0\rangle_A$, Alice rotates her cavity by applying X^{-A_1} . Next, Alice communicates her

measurement result to Bob. Since the value of the relative rotation, $u\Delta_c$, cannot be determined solely from A_1 and B_1 , Bob refers to a pre-calculated dictionary (see Appendix B) to determine the most likely value u_B . He then corrects the cavity state by applying $X^{-B_1+u_B\Delta_c}$, thereby optimizing the fidelity to the intermediate target state.

Modular number measurements – If the rotation was successful in correcting both types of angular misalignment, the state after completing the first stage can be rewritten in the dual basis as

$$L_{l_A}^A L_{l_B}^B \frac{1}{\sqrt{m_c}} \sum_{k=0}^{m_c-1} |k_+^{m_c}\rangle_A | -k_+^{m_c}\rangle_B \quad (9)$$

$$= \frac{1}{\sqrt{m_c}} \sum_{k=0}^{m_c-1} |(k-l_A)_+^{m_c}\rangle_A |(-k-l_B)_+^{m_c}\rangle_B, \quad (10)$$

with $|k_+^{m_c}\rangle \equiv \frac{1}{\sqrt{d/m_c}} \sum_{j=0}^{d/m_c-1} |(k+jm_c)_+\rangle$ representing a change in the modularity of the dual photon number basis from d to m_c . Equation (9) resembles the structure of the initial state in the computational basis, but with a negative sign in Bob's cavity (since the total photon number must be an integer multiple of m_c).

We will use this similarity in the second, loss correction stage, which is dual to the dephasing correction stage. Both parties measure the photon number modulo Δ_f as described by a set of PVMs $\{P_{x+}^{\Delta_f}\}_{x=0}^{x=\Delta_f-1}$, where x is the measurement result. Each PVM element can be written as

$$P_{x+}^{\Delta_f} = \sum_{j=0}^{d/\Delta_f-1} |(j\Delta_f+x)_+\rangle \langle(j\Delta_f+x)_+|. \quad (11)$$

This measurement determines the dimension $m_f \equiv \frac{m_c}{\Delta_f}$ of the subspace supporting the final qudit. Alice and Bob register their measurement outcomes as A_2 and B_2 , respectively. Alice then rotates her cavity in the dual basis by applying Z^{-A_2} , and sends her measurement outcome to Bob. Bob rotates his cavity in the dual basis by applying $Z^{-B_2-v_B\Delta_f}$, where $v_B\Delta_f$ is the most likely value for the relative misalignment determined using both outcomes and a second pre-calculated dictionary (Appendix B).

If the rotation in the second stage is successful, we obtain the desired target state

$$|\psi_t\rangle = \sum_{k=0}^{m_f-1} |(\Delta_f k)_+^{m_c}\rangle_A |(-\Delta_f k)_+^{m_c}\rangle_B. \quad (12)$$

As in the first stage, a rotation that does not successfully realign the states leads to an erroneous state and a reduced fidelity of the protocol. While the entanglement entropy of the target state $E_f = \log m_f < E_i$ is reduced by the protocol, we demonstrate in Section II E through numerical analysis that the fidelity of the distilled state to the ideal target state is significantly increased.

Conditional abort – The fidelity of the distilled state can be further improved by performing a final step in the protocol, which requires two-way communication. In this step, Bob calculates the expected fidelity conditioned on the measurement results $\mathcal{F}(A_1, B_1, A_2, B_2)$ and decides to abort the protocol if the result is lower than a pre-determined cut-off $f_{\text{cut}} \in \{0\} \cup [1/m_f^2, 1)$, where $1/m_f^2$ is the fidelity of the maximally mixed state. Setting a higher f_{cut} improves the average fidelity of the protocol but also increases the abort probability p_{abort} . Choosing $f_{\text{cut}} = 0$ corresponds to omitting this step, making two-way communication unnecessary. However, this choice also reduces the protocol's effectiveness (see Section II F).

We note that our protocol can be interpreted as a stabilizer-based entanglement distillation scheme [12], with a stabilizer group generated by $\langle Z^{m_c}, X^{d/m_f} \rangle$.

To benchmark the performance of the distillation protocol, we compare it to a scenario in which the parties do not communicate. The optimal strategy without relying on classical communication involves each party merging adjacent angular sections in phase space to reduce dephasing errors and merging adjacent dual-basis states to minimize loss errors (see Appendix C). This strategy effectively removes errors in redundant degrees of freedom and can, therefore, be interpreted as a form of error correction. We show in Section II E that the performance of our distillation protocol exceeds that of the no-communication protocol.

D. Four-level example

To illustrate the distillation procedure, we examine the protocol for a simplified model: a four-level system with $d = m_i = 4$. We choose $m_c = m_f = 2$, indicating that only the dephasing correction stage is applied. Therefore, we do not consider loss errors in this example and set $\gamma_l = 0$. The cut-off parameter is chosen to be $f_{\text{cut}} = 0.5$.

We consider the initial entangled state $|\psi_i\rangle = \frac{1}{\sqrt{4}} \sum_{i=0}^3 |k\rangle_A \otimes |k\rangle_B = \frac{1}{\sqrt{4}}(|00\rangle + |11\rangle + |22\rangle + |33\rangle)$, with $|kl\rangle \equiv |k\rangle_A \otimes |l\rangle_B$ (see Eq. (1)) and with initial entanglement entropy $E_i = 2$. The target state is $|\psi_t\rangle = \frac{1}{\sqrt{2}}(|00\rangle + |22\rangle)$, which has an entanglement entropy of $E_f = 1$. The state is affected by the dephasing channel \mathcal{N}_D and evolves to the noisy state (see Eq. (5))

$$\rho_{d=4} = p_0 |\psi_i\rangle \langle\psi_i| + p_1 |\varphi_+\rangle \langle\varphi_+| + p_1 |\varphi_-\rangle \langle\varphi_-| + p_2 |\varphi_0\rangle \langle\varphi_0|, \quad (13)$$

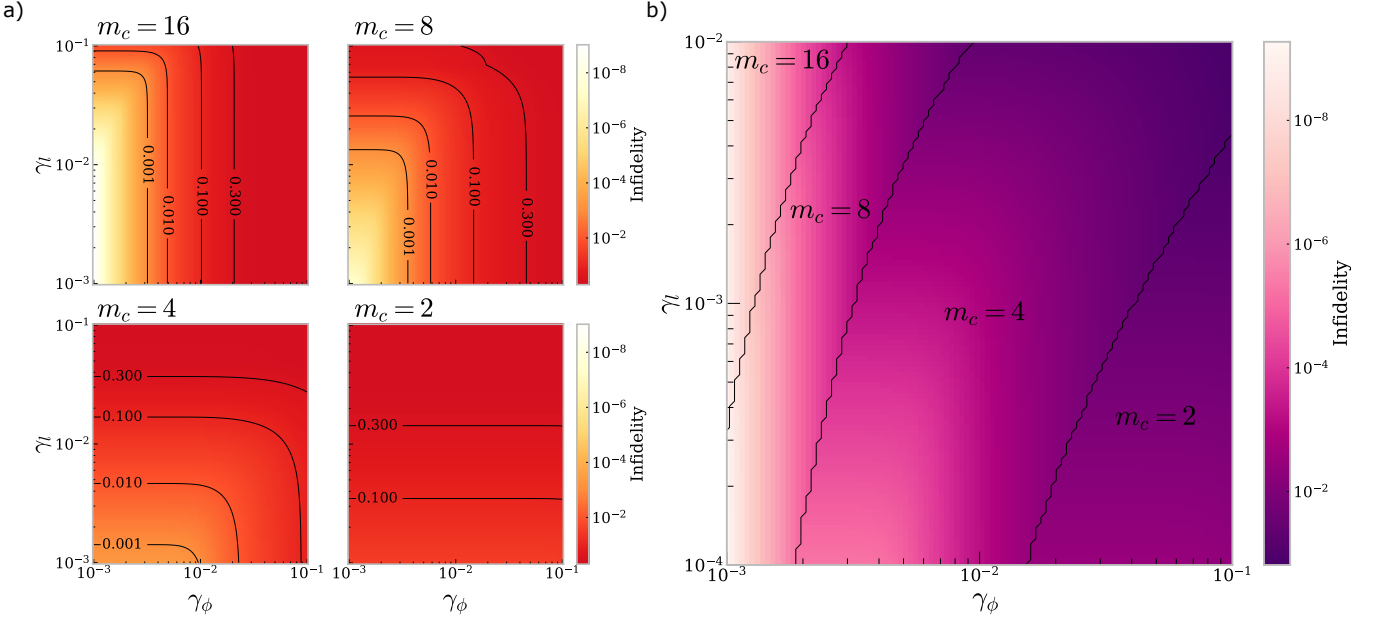


FIG. 4. Infidelity of the distilled state using the discrete model with initial qudit dimension $d = m_i = 16$ and average photon number $\bar{n} = 16$. **(a)** Infidelity as a function of both error rates γ_l and γ_ϕ for different intermediate qudit dimensions m_c . The results indicate that the distilled state fidelity is optimized by selecting different values of m_c for each error rate. **(b)** Infidelity of the distilled state when choosing the optimal m_c for each set of error rates γ_l and γ_ϕ . The black lines separate between regions with different optimal m_c .

where

$$\begin{aligned}
 |\varphi_+\rangle &= \frac{1}{\sqrt{4}} (|01\rangle + |12\rangle + |23\rangle + |30\rangle) \\
 &= D_B^1 |\psi_i\rangle = D_A^{-1} |\psi_i\rangle, \\
 |\varphi_-\rangle &= \frac{1}{\sqrt{4}} (|03\rangle + |10\rangle + |21\rangle + |32\rangle) \\
 &= D_A^1 |\psi_i\rangle = D_B^{-1} |\psi_i\rangle, \\
 |\varphi_o\rangle &= \frac{1}{\sqrt{4}} (|02\rangle + |13\rangle + |20\rangle + |31\rangle) \\
 &= D_A^{\pm 2} |\psi_i\rangle = D_B^{\pm 2} |\psi_i\rangle = D_B^1 D_A^{\mp 1} |\psi_i\rangle.
 \end{aligned}$$

The states $|\varphi_\pm\rangle$ are associated with a single dephasing error and occur with a probability p_1 (see Appendix II B). $|\varphi_o\rangle$ is the state after two dephasing errors, occurring with a probability p_2 . The probability of the system remaining in its initial state is denoted by $p_0 = 1 - 2p_1 - p_2$. We assume small error rates, such that $p_0 \gg p_1 \gg p_2$.

The parties next measure the modular phase, which, for $m_c = 2$, corresponds to a parity measurement in the computational basis. Alice and Bob record their outcomes as A_1 and B_1 , respectively.

If the parties obtain different parities, i.e., $A_1 \neq B_1$, they conclude that the original state was either $|\varphi_+\rangle$ or $|\varphi_-\rangle$ with equal probability. The party with the odd measurement result rotates its cavity (step 3 in Protocol 1), aligning it with the $|0\rangle$ state. The resulting, unnormalized, state is

$$\rho_{(A_1 \neq B_1)} = p_1 (|\widetilde{\varphi}_+\rangle \langle \widetilde{\varphi}_+| + |\widetilde{\varphi}_-\rangle \langle \widetilde{\varphi}_-|), \quad (14)$$

with $|\widetilde{\varphi}_+\rangle = \frac{1}{\sqrt{2}}(|00\rangle + |22\rangle) = |\psi_t\rangle$ and $|\widetilde{\varphi}_-\rangle = \frac{1}{\sqrt{2}}(|02\rangle + |20\rangle)$. When obtaining these measurement outcomes, the two parties conclude that the fidelity of the final state relative to the target state is 0.5, which is equal to f_{cut} . Therefore, Alice and Bob abort the protocol.

In contrast, for $A_1 = B_1$, the measured state must have originated from either $|\psi_i\rangle$ or $|\varphi_o\rangle$. When both outcomes are even, i.e., $A_1 = B_1 = 0$, the systems are already aligned with $|0\rangle$ and the parties do not need to perform rotations. For $A_1 = B_1 = 1$, the parties rotate their cavities to realign their states with the $|0\rangle$ state. In either scenario, the final state is

$$\sigma_f = p_0 |\psi_t\rangle \langle \psi_t| + p_2 |\widetilde{\varphi}_o\rangle \langle \widetilde{\varphi}_o|, \quad (15)$$

where $|\widetilde{\varphi}_o\rangle = \frac{1}{\sqrt{2}}(|02\rangle + |20\rangle)$. The fidelity of the distilled state to the desired target state $|\psi_t\rangle$ is therefore $\frac{p_0}{(p_0 + p_2)}$.

Due to the super-exponential nature of the noise channel, we obtain $p_2 \ll p_1^2$. This unique feature of bosonic noise leads to a much more efficient suppression of errors with the bosonic distillation protocol compared to the corresponding qubit distillation protocols.

We next benchmark the distillation protocol performance by comparing it to the no-communication protocol. Merging adjacent angular sections in phase space effectively coarse-grains the qudits to qubits. In the case of a traditional distillation protocol using two Bell pairs of qubits, this procedure is equivalent to discarding one of the Bell pairs. The coarse-graining procedure results in a fidelity to the target state of $1 - p_1 - p_2$, which is lower than

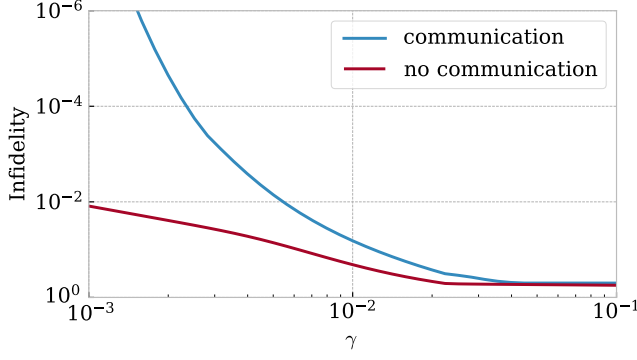


FIG. 5. Infidelity of the distilled state when performing the protocol with communication (blue line) and without communication (red line), with $m_i = 16, m_f = 2, \bar{n} = 49$ and $\gamma = \gamma_l = \gamma_\phi$. In the distillation protocol, we maximize the fidelity by choosing the optimal m_c , whereas in the no-communication protocol, the optimal rotation strategy is chosen for each error rate.

our distillation protocol fidelity when $p_2 < \frac{1}{2}(1 - 2p_1)$. This inequality holds for the regime of interest, in which $p_0 \gg p_1 \gg p_2$.

E. Performance of the protocol

Next, we numerically analyze the performance of the protocol for higher-dimensions, where analytical derivations become impractical. In Figure 4a, we show the simulated infidelity between the distilled state and the target state as a function of the loss and dephasing rates γ_l, γ_ϕ . We plot the infidelity for four different values of the intermediate dimension parameter, m_c , assuming $m_i = d = 16$ and $m_f = 2$. We also choose $f_{\text{cut}} = 0$, meaning the protocol is never aborted.

We observe that when the dephasing rate is dominant, smaller values of m_c yield a higher fidelity (see 4b). Conversely, when loss errors dominate, choosing a larger m_c improves the fidelity. This behavior can be explained by noting that a smaller m_c increases the separation between angular sections supporting the state after the first distillation stage, corresponding to a higher tolerance to dephasing errors. When loss is dominant, choosing a higher m_c increases the separation in the dual basis after the second distillation stage, increasing the robustness to loss errors.

The trade-off between loss and dephasing distillation can also be understood by noting that the first distillation stage maps the state from a space of dimension m_i^2 to a subspace of dimension m_c^2 to correct dephasing errors, followed by a map to a subspace of dimension m_f^2 to correct loss errors. This is akin to distilling the entanglement of $\log m_i$ qubit pairs in traditional multi-qubit distillation to $\log m_c$ qubit pairs and then to $\log m_f$ qubit pairs in a second step. This comparison suggests that m_c controls the balance between the two stages, allowing us to optimize the final fidelity. In Figure 4b, we show the highest

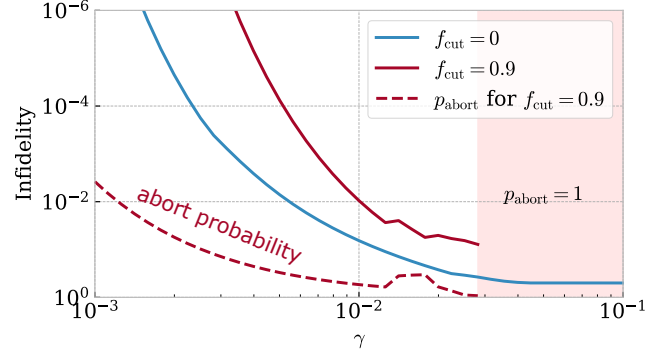


FIG. 6. Infidelity of the distilled state when performing the protocol with abort criterion (red line, $f_{\text{cut}} = 0.9$) and without abort criterion (blue line, $f_{\text{cut}} = 0$), for $d = 32, m_i = 16, m_f = 2, \bar{n} = 49$ and $\gamma_l = \gamma_\phi = \gamma$. In both scenarios, we set m_c to optimize the fidelity. This can lead to non-monotonic behavior of the abort probability (dashed line). The non-monotonic behavior of the infidelity is due to low-fidelity states passing the cut-off as γ decreases, thereby increasing the average infidelity. The shaded region indicates error rates where the fidelity is below f_{cut} for all instances of the protocol.

achievable fidelity for each pair (γ_l, γ_ϕ) by maximizing over m_c .

As discussed in Section II C, we can evaluate the performance of the distillation protocol by comparing it to a no-communication strategy. In this approach, the parties must agree on a predetermined strategy in advance, where each party applies operations to their cavity based solely on their own measurement outcomes. Figure 5 compares the infidelity for both strategies, showing that the distillation protocol outperforms the no-communication strategy across the considered parameters.

The protocol can also be used to distill states with higher final entanglement entropy. To achieve this, we can set the final cavity state dimension, m_f , to be greater than two at the cost of a reduction in the protocol fidelity. The performance of this scenario is analyzed in Appendix D.

F. Aborting the distillation protocol

To enhance the distillation fidelity, the parties restart the protocol based on the expected fidelity conditioned on the measurement outcomes $\mathcal{F}(A_1, B_1, A_2, B_2)$. This approach requires two-way communication instead of one-way communication and comes at the cost of a reduced success probability $1 - p_{\text{abort}}$.

In Figure 6, we compare the average infidelity of the distilled state under different abort criteria $\mathcal{F}(A_1, B_1, A_2, B_2) \leq f_{\text{cut}}$ for $f_{\text{cut}} = 0.9$ and $f_{\text{cut}} = 0$, the latter indicating that the protocol is never aborted. The option to abort becomes particularly effective when the qudit dimension d is increased while keeping m_i fixed. By partitioning the cavity phase space into more sections,

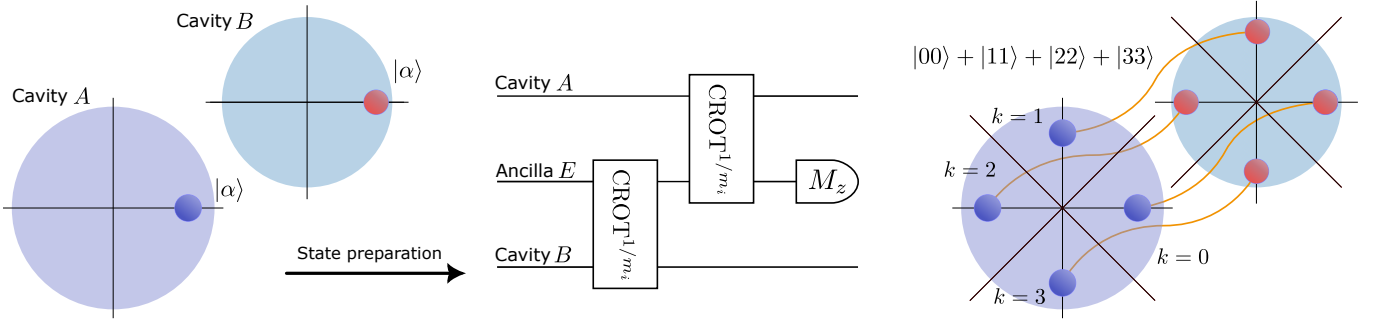


FIG. 7. Schematic representation of the entangled state preparation process. We start with two non-entangled cavities, each prepared in an initial primitive state $|\Theta\rangle$, here represented by a coherent state $|\alpha\rangle$. The state preparation includes the introduction of an ancilla cavity E and the application of two CROT^{1/m_i} gates. The ancilla is then measured, leaving us with an entangled two-cavity state depicted on the right. The entanglement entropy of the final state is $E_i = \log(m_i)$. In this example, we use $m_i = d = 4$.

we effectively increase the measurement resolution, enabling us to more accurately determine when to abort the protocol, thereby improving performance. Therefore, we do not assume $d = m_i$ in Figure 6. The probability of aborting the protocol is also shown, emphasizing the trade-off between the achievable fidelity of the distilled state and the probability of successful distillation.

III. IMPLEMENTING THE PROTOCOL USING BOSONIC SYSTEMS

A. Preparing the initial state

We now detail the procedure for initializing the entangled qudit state given in Eq. (1) in a two-cavity system. This involves translating the discrete qudit description used thus far into bosonic states described by continuous variables. Our starting point is a product state of the two cavities, each prepared in a primitive state $|\Theta\rangle$ that is approximately localized in one angular section of the cavity phase space.

The qudit basis can be constructed from rotated primitive states

$$|k^{\text{CV}}\rangle \equiv R_{2k\pi/m_i} |\Theta\rangle, \quad (16)$$

where $R_\theta \equiv e^{i\theta\hat{n}}$ is the phase-space rotation operator with θ the rotation angle and \hat{n} the number operator.

To create the highly entangled initial state with entanglement entropy $\log_2 m_i$, we use a modified version of the controlled rotation (CROT) gate introduced in Ref. [21],

$$\text{CROT}^{1/m_i} := e^{i\frac{2\pi}{m_i}\hat{n}_A\hat{n}_B},$$

with $\hat{n}_{A(B)}$ the number operator of the mode in cavity $A(B)$.

This gate can be implemented by applying a coupling Hamiltonian $\hat{n}_A\hat{n}_B$ for a duration of $\frac{2\pi}{m_i}$. Counterintuitively, the entanglement generated by the gate increases

as the gate duration decreases. Furthermore, this shorter duration can also reduce the infidelity of the entangled state.

The initialization protocol uses an ancilla cavity E in addition to cavities A and B (Fig. 7). We initialize all three cavities in $|0^{\text{CV}}\rangle$ and apply two CROT^{1/m_i} gates, once between cavities A and E and once between cavities B and E . We then measure the ancilla in its logical Z basis, and register the result as x .

We choose the primitive state such that the states $|k^{\text{CV}}\rangle$ are approximately orthogonal. Under this condition, the procedure creates a channel \mathcal{C}_x that acts on the initial state as (Appendix F)

$$\begin{aligned} \mathcal{C}_x(|0^{\text{CV}}\rangle_A |0^{\text{CV}}\rangle_B |0^{\text{CV}}\rangle_E) \\ = \frac{1}{\sqrt{m_i}} \sum_{k=0}^{m_i-1} e^{-2ikx\pi/m_i} |k^{\text{CV}}\rangle_A |k^{\text{CV}}\rangle_B \\ = Z_A^{-x} \frac{1}{\sqrt{m_i}} \sum_{k=0}^{m_i-1} |k^{\text{CV}}\rangle_A |k^{\text{CV}}\rangle_B. \end{aligned} \quad (17)$$

Finally, applying a local unitary Z_A^x (or accounting for it in software) leaves us with the desired initial entangled state $|\psi_\Theta\rangle = \frac{1}{\sqrt{m_i}} \sum_{k=0}^{m_i-1} |k^{\text{CV}}\rangle_A |k^{\text{CV}}\rangle_B$.

A similar entangled state can be prepared using only a single CROT^{1/m_i} gate between Alice's and Bob's cavities, without the need for an ancilla cavity. The resulting state $\frac{1}{\sqrt{m_i}} \sum_{k=0}^{m_i-1} |k^{\text{CV}}\rangle_A |k_+^{\text{CV}}\rangle_B$ is similar to $|\psi_\Theta\rangle$, but with one of the cavities transformed to the dual basis. This state can be distilled using a similar protocol, where one of the parties acts in the dual basis while the other acts in the computational basis during the first stage, and vice-versa during the second stage.

B. Continuous-variable description of the distillation protocol

To describe the protocol in a continuous-variable framework, we proceed to redefine the operations introduced in Section II C as completely positive maps from the bosonic space onto itself.

We first define the angular section (logical Z) measurement as a set of POVMs [21, 33]

$$M_k = \frac{1}{\pi} \sum_{m,n=0}^{\infty} \Gamma_{m,n}^k |m\rangle \langle n|, \quad (18)$$

where $k \in \{0, \dots, d-1\}$ is the outcome corresponding to the k^{th} angular section, $|m\rangle$ and $|n\rangle$ are the Fock-space basis states, and $\Gamma_{m,n}^k$ are coefficients described in Appendix F. Here, d determines the phase measurement resolution.

The Δ_c -modular phase measurement with outcome $x \in \{0, \dots, \Delta_c - 1\}$ is defined analogously to Eq. (7) as

$$P_x^{\Delta_c} = \sum_{n=0}^{m_c-1} M_{n\Delta_c+x}, \quad (19)$$

with $m_c = d/\Delta_c$.

This modular phase measurement can be implemented by applying an interaction Hamiltonian $a^{m_c} r^\dagger + \text{h.c.}$, where a and r are the annihilation operators of the measured mode and a buffer mode, respectively. The phase obtained from a heterodyne measurement of the field leaking from the buffer mode corresponds to the phase of the cavity state modulo $2\pi/m_c$. This procedure may be accompanied by autonomous stabilization techniques to maintain the average photon number in the measured mode throughout the measurement process [34].

The completely positive map that corresponds to the parties measuring the results A_1 and B_1 , is $\mathcal{P}^{A_1, B_1}(\bullet) = P_{A_1}^{\Delta_c} \otimes P_{B_1}^{\Delta_c} \bullet P_{A_1}^{\Delta_c} \otimes P_{B_1}^{\Delta_c}$. To correct the dephasing errors, Alice and Bob rotate their cavities by $-A_1 2\pi/d$ and $(-B_1 + u_B \Delta_i) 2\pi/d$ (see Protocol 1), corresponding to the unitary map

$$\mathcal{U}_{A_1, B_1}^\phi(\bullet) = R_{-A_1 2\pi/d}^A \otimes R_{(-B_1 + u_B) 2\pi/d}^B \bullet R_{-A_1 2\pi/d}^{A\dagger} \otimes R_{(-B_1 + u_B) 2\pi/d}^{B\dagger}. \quad (20)$$

The Δ_f -modular measurements of the photon number (see Eq. (11)), which correspond to measuring the qudit in its dual basis, can be expressed as

$$P_{x+}^{\Delta_f} = \sum_{j=0}^{\infty} |x + j\Delta_f\rangle \langle x + j\Delta_f|, \quad (21)$$

where $|x + j\Delta_f\rangle$ are the Fock-space basis states, and $x \in \{0, \dots, \Delta_f - 1\}$ is the measurement outcome. Methods for implementing modular photon number measurements are

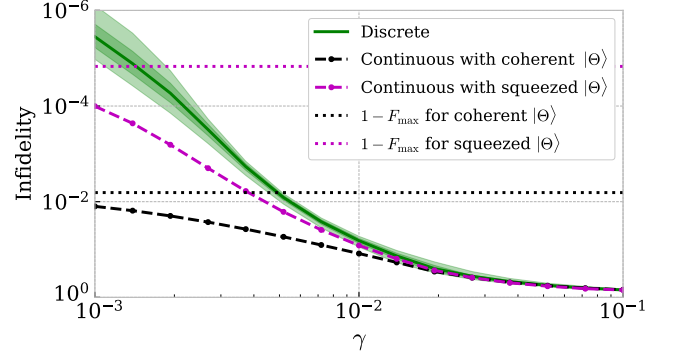


FIG. 8. Simulated infidelity of the final distilled state as a function of the loss and dephasing rates with $\gamma_l = \gamma_\phi = \gamma$. We compare the discrete model with $\bar{n} = 49$ (solid green line) to the continuous-variable model for a coherent primitive state $|\Theta\rangle = |\alpha = 7\rangle$ (dashed black line) and a squeezed primitive state $|\Theta\rangle = |\alpha = 7, \zeta = -0.8\rangle$ (dashed magenta line), with α and ζ the amplitude and squeezing parameters, respectively. The shaded areas represent the discrete model with photon number $\bar{n} \pm \Delta n$ to account for the photon number uncertainty of the coherent (dark green, $\Delta n = 7$) and squeezed (light green, $\Delta n = 15.7$) primitive states. For all cases, we use $m_i = d = 16, m_c = 8, m_f = 2$.

described in Refs. [21, 35, 36]. The map corresponding to the parties obtaining outcomes A_2 and B_2 is $\mathcal{P}_+^{A_2, B_2}(\bullet) = P_{A_2+}^{\Delta_f} \otimes P_{B_2+}^{\Delta_f} \bullet P_{A_2+}^{\Delta_f} \otimes P_{B_2+}^{\Delta_f}$.

Compensating for photon loss errors by adding photons to a cavity is a non-trivial operation [37]. Therefore, it is more practical to account for the measurement outcomes in software. Depending on these outcomes, the distilled entangled state may differ from the original target state. Consequently, when evaluating the distilled state fidelity, we adjust the target state accordingly to reflect the actual state produced.

When applying the concatenation of all the aforementioned channels to the initial state $|\psi_\Theta\rangle$ (subsection III A), the distillation protocol results in the final state

$$\rho = \sum_{A_1, A_2, B_1, B_2} \mathcal{P}_+^{A_2, B_2} \circ \mathcal{U}_\phi^{A_1, B_1} \circ \mathcal{P}^{A_1, B_1} \circ \mathcal{N}(|\psi_\Theta\rangle \langle \psi_\Theta|), \quad (22)$$

where the sum runs over all possible measurement outcomes and \mathcal{N} represents the loss-dephasing channel (see Appendix A 1).

C. Comparison between discrete and continuous descriptions

The discrete qudit model outlined in section II B provides a convenient framework for describing the distillation protocol. However, it overlooks certain features of bosonic systems, such as the nonzero overlap between primitive states associated with different angular sections.

The overlap between a primitive state $|\Theta\rangle$ and the k^{th} section can be quantified as

$$\delta_k \equiv \langle \Theta | M_k | \Theta \rangle , \quad (23)$$

where M_k is the POVM defined in Eq. (18).

Therefore, even in the absence of loss-dephasing noise, the state can be detected in sections other than the initial one, which can be interpreted as a result of quantum noise.

In the first stage of the protocol, a dephasing error of more than $\lceil \Delta_c/2 \rceil$ sections in either direction results in an unsuccessful correction. We can use this understanding to bound the protocol infidelity due to the overlap with other sections by

$$1 - F_{\max} = 2\delta_{\lceil \Delta_c/2 \rceil} . \quad (24)$$

This limitation of the protocol can be mitigated for a coherent primitive state by increasing its amplitude or by squeezing it along the radial axis, thereby reducing the overlap with adjacent sections. However, this comes at the expense of increased photon loss.

Another approximation made in the discrete model is a heuristic photon-loss noise model (Appendix A 2) that uses the average photon number \bar{n} without considering the photon number distribution. This distinction is particularly relevant for primitive states with large photon-number uncertainty, such as squeezed states.

To evaluate the accuracy of the discrete model, we compare the protocol performance using this model to the numerically simulated infidelity obtained with the continuous-variable model for coherent and squeezed primitive states (see Fig. 8). To evaluate the distillation infidelity we use a decoding map \mathcal{D} from the continuous-variable bosonic Hilbert space to a d -dimensional logical Hilbert space (Appendix G).

To highlight the effect of the photon number uncertainty, we also show the discrete model infidelity for $\bar{n} \pm \Delta n$, where Δn is the standard deviation of the photon number distribution.

The numerical results indicate that the discrete model provides a good approximation when the protocol infidelity exceeds the error introduced by quantum noise. For sufficiently low loss and dephasing error rates, the continuous-variable model predicts that the fidelity of the distilled state saturates to the quantum noise limit. Reducing the effect of quantum noise by squeezing a coherent primitive state significantly enhances the achievable distillation fidelity.

IV. CONCLUSION

We have introduced an entanglement distillation procedure for bosonic systems using states with discrete rotation symmetry in phase space. This choice ensures compatibility with the rotation-symmetric bosonic quantum error correction codes introduced in Ref. [21]. In particular, the final distilled state with $m_f = 2$ corresponds to an encoded Bell state, which can be used in bosonic fault-tolerant quantum computing schemes [21] and facilitates distributed bosonic quantum computing [38].

Additionally, our distillation protocol can be extended to other bosonic encodings. For instance, by using initial entangled states with translation symmetry in phase space instead of rotation symmetry, the distillation protocol becomes compatible with GKP (grid) quantum error correcting codes [17, 26, 27, 32]. In this case, angular rotations and photon addition are replaced with more straightforward displacements along the position and momentum coordinates. Since our bosonic distillation protocol is limited to a single-shot application, concatenation with a traditional distillation protocol at the logical level could be used to achieve even higher fidelities.

In this work, we assumed that the noise channel only impacts the transmission step between Alice and Bob. Future work should address additional sources of errors, including those arising during state preparation and measurement, as well as cavity non-linearity resulting from high photon-number populations. We expect the distillation procedure to remain robust against these errors, as these operations typically induce loss and dephasing errors, which the procedure is designed to correct.

Our proposed distillation scheme relies on operations native to bosonic systems, with many of the required building blocks [25, 37, 39–41] and quantum links [42–46] already demonstrated in recent hardware. We therefore anticipate that this protocol can be realized using currently available experimental platforms.

ACKNOWLEDGMENTS

The authors thank Liang Jiang for his helpful comments on this manuscript. All authors acknowledge support from the Marshall and Arlene Bennett Family Research Program. SJ and SR acknowledge additional financial support from the Israel Science Foundation ISF Quantum Science and Technologies Grants No. 963/19 and No. 2022/20, and the European Research Council Starting Investigator Grant No. Q-CIRC 101040179. RAF research was also generously supported by the Peter and Patricia Gruber Award and the Koshland Research Fund. SR is the incumbent of the Rabbi Dr Roger Herst Career Development Chair and RAF holds the Daniel E. Koshland Career Development Chair.

Appendix A: Error probabilities of the discrete model

1. The loss-dephasing channel

The main noise sources in bosonic systems are photon loss and dephasing. The density matrix ρ of such a system evolves under the combined loss and dephasing channels [32] according to the master equation

$$\dot{\rho} = \kappa_l \mathcal{D}[\hat{a}]\rho + \kappa_\phi \mathcal{D}[\hat{n}]\rho, \quad (\text{A1})$$

where \hat{a} and \hat{n} are the annihilation and number operators of the bosonic system, κ_l and κ_ϕ are the loss and dephasing rates, and $\mathcal{D}[\hat{A}]$ is the Lindbladian defined as

$$\mathcal{D}[\hat{A}](\bullet) = \hat{A} \bullet \hat{A}^\dagger - \frac{1}{2} \hat{A}^\dagger \hat{A} \bullet - \frac{1}{2} \bullet \hat{A}^\dagger \hat{A}. \quad (\text{A2})$$

with \bullet denoting any linear operator over the bosonic system's Hilbert space.

This allows us to define the loss-dephasing channel as the time evolution superoperator

$$\mathcal{N}[\kappa_l, \kappa_\phi] = e^{\kappa_l t \mathcal{D}[\hat{a}] + \kappa_\phi t \mathcal{D}[\hat{n}]}, \quad (\text{A3})$$

with t the evolution time and $\rho(t) = \mathcal{N}[\kappa_l, \kappa_\phi](\rho(0))$. Since the loss and dephasing channels commute, we can decompose the combined channel into two independent channels $\mathcal{N}[\kappa_l, \kappa_\phi] = \mathcal{N}_L[\gamma_l \equiv 1 - e^{-\kappa_l t}] \circ \mathcal{N}_D[\gamma_\phi \equiv \kappa_\phi t]$. These separate channels can be written using the Kraus-operator representation as [32]

$$\mathcal{N}_L[\gamma_l] = \sum_{k=0}^{\infty} \hat{L}_k \bullet \hat{L}_k^\dagger, \quad \hat{L}_k = \sqrt{\frac{\gamma_l^k}{k!}} (1 - \gamma_l)^{\hat{n}/2} \hat{a}^k \quad (\text{A4})$$

$$\mathcal{N}_D[\gamma_\phi] = \frac{1}{\sqrt{2\pi\gamma_\phi}} \int_{-\infty}^{\infty} e^{-\frac{\phi^2}{2\gamma_\phi}} R_\phi \bullet R_\phi^\dagger d\phi. \quad (\text{A5})$$

2. Discretized errors

Using the channels described above, we can construct an approximate error model for the discretized system introduced in Section II B.

The dephasing channel can be interpreted using Eq. (A5) as a statistical mixture of phase-space rotations by an angle ϕ with a Gaussian probability distribution:

$$f_D(\phi) = \frac{1}{\sqrt{2\pi\gamma_\phi}} e^{-\frac{\phi^2}{2\gamma_\phi}}. \quad (\text{A6})$$

We discretize the dephasing errors by approximating rotations within the angular interval $\phi \in ((2s-1)\pi/d, (2s+1)\pi/d)$ as a discrete dephasing error by s sections. The corresponding probability for dephasing by s sections is:

$$p_s^D = \int_{(2s-1)\pi/d}^{(2s+1)\pi/d} f_D(\phi) d\phi = \frac{1}{2} \left[\text{erf} \left(\sqrt{\frac{1}{2\gamma_\phi}} (2s+1)\pi/d \right) - \text{erf} \left(\sqrt{\frac{1}{2\gamma_\phi}} (2s-1)\pi/d \right) \right],$$

with erf the error function.

The probability of losing l photons depends on the photon number distribution of the bosonic state. For approximating the loss probability in the discrete model, we assume that the photon number distribution is sharply peaked around the average photon population \bar{n} . Using Eq. (A4), we can therefore write

$$\tilde{p}_l^L = \langle \hat{L}_l^\dagger \hat{L}_l \rangle \approx \frac{\gamma_l^l}{l!} (1 - \gamma_l)^{\bar{n}} \bar{n}^l. \quad (\text{A7})$$

The sum of the loss probabilities $p_l^L(\bar{n})$ does not necessarily equal 1. Thus, we normalize them as follows:

$$p_l^L = \frac{\tilde{p}_l^L}{\sum_{j \geq 0} \tilde{p}_j^L}. \quad (\text{A8})$$

We plot the discrete error probabilities in Fig. A2. This distribution exhibits super-exponential decay, which distinguishes it from typical qubit-based distillation protocols. As a result, we observe that $p_{s=2}^D \ll p_{s=1}^D{}^2$.

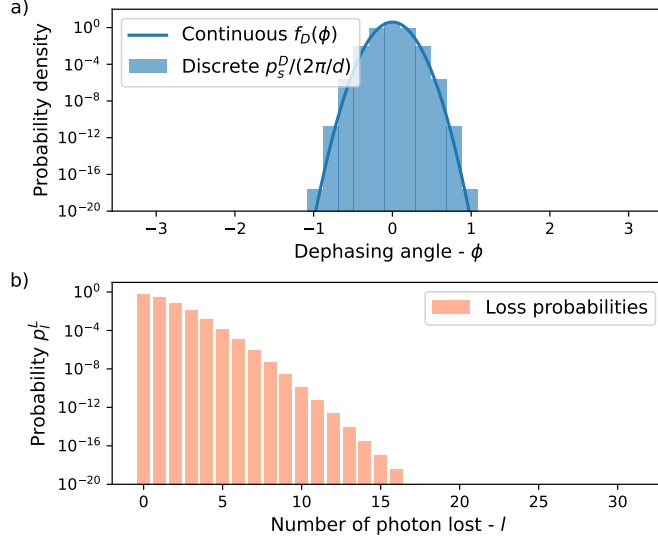


FIG. 9. a) Probability density of dephasing by an angle ϕ without the discrete approximation ($f_D(\phi)$, solid line) and with the discrete approximation ($p_s^D/(2\pi/d)$, bars), $\gamma_\phi = 10^{-2}$. b) Probability of losing l photons with the discrete approximation. Here, $\bar{n} = 49$ and $\gamma_l = 10^{-2}$.

Appendix B: Analyzing the distillation protocol

In order to calculate the fidelity of the distilled state, we follow the system's density matrix from the initial noisy entangled state through the measurements and the corrections by the parties. In the appendices, we do not assume $m_i = d$.

The initial state is described by Eq. (5) in the main text as follows:

$$\rho = \sum_{\bar{x} \in \mathcal{E}} p(\bar{x}) |\varphi_{\bar{x}}\rangle \langle \varphi_{\bar{x}}|, \quad (\text{B1})$$

where $|\varphi_{\bar{x}}\rangle = L_{l_A}^A L_{l_B}^B D_{s_A}^A D_{s_B}^B |\psi_i\rangle$ are the error states associated with the error $\bar{x} = (s_A, s_B, l_A, l_B)$. The summation is over all possible errors. Since the initial state ψ_i can be considered as the state corresponding to $\bar{x} = (0, 0, 0, 0)$, we hereafter include it in the summation. Writing the error states explicitly, we have:

$$|\varphi_{\bar{x}}\rangle = L^{l_A} L^{l_B} \sum_{k=0}^{m_i-1} |\Delta_i k + s_A\rangle_A |\Delta_i k + s_B\rangle_B, \quad (\text{B2})$$

with $\Delta_i = d/m_i$.

In the first distillation stage, which corrects dephasing errors, both parties perform modular- Δ_c phase measurements, yielding outcomes A_1 and B_1 for Alice and Bob, respectively. When applying the PVM (Eq. (7) in the main text)

$$P_x^{\Delta_c} = \sum_{j=0}^{d/\Delta_c-1} |j\Delta_c + x\rangle \langle j\Delta_c + x| \quad (\text{B3})$$

to the error state $|\varphi_{\bar{x}}\rangle$, we obtain:

$$|\tilde{\varphi}_{\bar{x}}\rangle \equiv P_{A_1}^{\Delta_c} P_{B_1}^{\Delta_c} |\varphi_{\bar{x}}\rangle = \frac{L^{l_A} L^{l_B}}{\sqrt{m_i}} \left(\sum_{n,m=0}^{d/\Delta_c-1} |\Delta_c n + A_1\rangle_A \langle \Delta_c n + A_1|_A \otimes |\Delta_c m + B_1\rangle_B \langle \Delta_c m + B_1|_B \right) \sum_{k=0}^{m_i-1} |\Delta_i k + s_A\rangle_A |\Delta_i k + s_B\rangle_B. \quad (\text{B4})$$

For the projection to be non-zero, the inner products $\langle \Delta_c n + A_1 |_A | \Delta_i k + s_A \rangle_A$ and $\langle \Delta_c m + B_1 |_B | \Delta_i k + s_B \rangle_B$ must be non-zero for certain values of (n, k, m) . This occurs only under the constraints:

$$A_1 = s_A \pmod{\Delta_i}, \quad (\text{B5})$$

$$B_1 = s_B \pmod{\Delta_i}, \quad (\text{B6})$$

$$A_1 - B_1 = s_A - s_B \pmod{\Delta_c}. \quad (\text{B7})$$

resulting in the post-measurement state described by Eq. (8):

$$|\tilde{\varphi}_{\bar{x}}\rangle = \frac{1}{\sqrt{m_c}} \sum_{k'=0}^{m_c-1} c_{k'} |\Delta_c k' + A_1\rangle_A |\Delta_c k' + \Delta_c u + B_1\rangle_B, \quad (\text{B8})$$

with $c_{k'}$ a phase factor resulting from possible loss errors and $u = \frac{\delta_s + A_1 - B_1}{\Delta_c}$ an integer.

Considering the full density matrix again (Eq. (B1)), the constraints (B5)–(B7) can also be used to reduce the possible set of errors \mathcal{E} , yielding the post-measurement density matrix

$$\rho_1 = \sum_{\bar{x} \in \mathcal{E}_1} p(\bar{x}) |\tilde{\varphi}_{\bar{x}}\rangle \langle \tilde{\varphi}_{\bar{x}}|, \quad (\text{B9})$$

$$\mathcal{E}_1 = \left\{ \bar{x} = (s_A, s_B, l_A, l_B) \in \mathcal{E} : \begin{array}{l} s_A = A_1 \pmod{\Delta_i} \\ s_B = B_1 \pmod{\Delta_i} \\ s_A - s_B = A_1 - B_1 \pmod{\Delta_c} \end{array} \right\}. \quad (\text{B10})$$

We next describe the phase-space rotations that Alice and Bob must apply to realign their states with the $|0\rangle$ state of their respective cavities and to realign the cavities with respect to each other.

Alice's phase-space rotation is based solely on her measurement outcome A_1 . She realigns her state with the $|0\rangle$ state by applying X^{-A_1} . Bob's rotation, on the other hand, depends on both his own result and Alice's. He calculates an integer u_B that maximizes the probability of a successful realignment using a rotation $X^{-B_1 + u_B \Delta_c}$.

After the application of these phase-space rotations, the error state can be written as

$$|\tilde{\varphi}'_{\bar{x}}\rangle = \frac{1}{\sqrt{m_c}} L^{l_A} L^{l_B} \sum_{k=0}^{m_c-1} |\Delta_c k\rangle_A |\Delta_c k + s_B - s_A + A_1 - B_1 + u_B \Delta_c\rangle_B \quad (\text{B11})$$

$$= \frac{1}{\sqrt{m_c}} L^{l_A} L^{l_B} \sum_{k=0}^{m_c-1} |\Delta_c k\rangle_A |\Delta_c (k + u + u_B)\rangle_B. \quad (\text{B12})$$

This equation indicates that the condition for a successful rotation is

$$u = -u_B \pmod{m_c}. \quad (\text{B13})$$

In order to maximize the probability for a successful realignment, we find the value of u that maximizes the likelihood $\mathcal{L}(u|A_1, B_1)$ [47]. Since the probability for a specific error \bar{x} is $p(\bar{x}) = p_{s_A}^D p_{s_B}^D p_{l_A}^L p_{l_B}^L$, we can sum over all the different possible errors \bar{x} that result in measurement outcomes (A_1, B_1) . The dephasing errors that satisfy the constraints from Eq. (B10) can be expressed as $s_A = A_1 + t\Delta_i$ and $s_B = B_1 + t\Delta_i + u\Delta_c$, where $t, u \in \mathbb{Z}$. Thus, we obtain

$$u_B = -\arg \max_{u \in \mathbb{Z}} \left(\sum_{t=0, \pm 1, \dots} p_{A_1+t\Delta_i}^D \cdot p_{B_1+t\Delta_i+u\Delta_c}^D \right). \quad (\text{B14})$$

The loss probabilities do not affect the calculation and are therefore omitted from this expression.

The second stage, in which loss errors are corrected, can be better understood by examining the error state from Eq.

(B11) in the dual basis:

$$\begin{aligned}
|\tilde{\varphi}'_{\bar{x}}\rangle &= \frac{\hat{P}}{\sqrt{m_c}} \sum_{k=0}^{m_c-1} |\Delta_c k\rangle_A |\Delta_c k\rangle_B = \frac{\hat{P}}{\sqrt{m_c}} \sum_{k=0}^{m_c-1} \left(\frac{1}{\sqrt{d}} \sum_{j=0}^{d-1} e^{-2ij\Delta_c k\pi/d} \cdot |j_+\rangle \right) \left(\frac{1}{\sqrt{d}} \sum_{t=0}^{d-1} e^{-2it\Delta_c k\pi/d} \cdot |t_+\rangle \right) \\
&= \frac{\hat{P}}{\sqrt{m_c d}} \sum_{j,t=0}^{d-1} \sum_{k=0}^{m_c-1} e^{-2i(j+t)\Delta_c k\pi/d} |j_+\rangle_A |t_+\rangle_B = \frac{\hat{P}}{\sqrt{m_c d}} \sum_{j,t=0}^{d-1} \left(\sum_{k=0}^{m_c-1} e^{-2i(j+t)k\pi/m_c} \right) |j_+\rangle_A |t_+\rangle_B \\
&= \frac{\hat{P}}{\sqrt{m_c d}} \sum_{j,t=0}^{d-1} \left(m_c \sum_{u=-\infty}^{\infty} \delta_{j,-t+m_c \cdot u} \right) |j_+\rangle_A |t_+\rangle_B = \frac{\hat{P}}{\sqrt{m_c \Delta_c}} \sum_{t=0}^{d-1} \sum_{u=0}^{\Delta_c} |(-t + m_c \cdot u)_+\rangle_A |t_+\rangle_B \\
&= \frac{\hat{P}}{\sqrt{m_c \Delta_c}} \sum_{t=0}^{d-1} |-t_+^{m_c}\rangle_A |t_+\rangle_B = \frac{\hat{P}}{\sqrt{m_c}} \sum_{t=0}^{m_c-1} |-t_+^{m_c}\rangle_A |t_+^{m_c}\rangle_B .
\end{aligned}$$

Here, $\hat{P} = L_{l_A}^A L_{l_B}^B D_{(u-u_B)\Delta_c}^B$ represents the residual error operator. Specifically, the dephasing operator $D_{(u-u_B)\Delta_c}^B$ represents an unsuccessful correction in the first stage. Because any states with $u \neq u_B$ are orthogonal to the desired state – and thus do not contribute to the fidelity – we later omit them from the density matrix (without renormalization). Consequently, we can continue analyzing the protocol without including this dephasing operator. Thus, we recover Eq. (10) in the main text:

$$\frac{1}{\sqrt{m_c}} \sum_{k=0}^{m_c-1} |(k - l_A)_+^{m_c}\rangle_A |(-k - l_B)_+^{m_c}\rangle_B . \quad (\text{B15})$$

The second stage of the protocol starts with both parties performing a modular measurement in the dual basis. Alice and Bob register the results as A_2 and B_2 , respectively. Acting on the error state with the PVMs (first introduced in Eq. (11) in the main text)

$$P_{x+}^{\Delta_f} = \sum_{j=0}^{d/\Delta_f-1} |(j\Delta_f + x)_+\rangle \langle (j\Delta_f + x)_+| , \quad (\text{B16})$$

we can deduce that the state after the dual-basis measurement meets the constraint

$$l_A + l_B = -(A_2 + B_2) \pmod{m_c/m_f} . \quad (\text{B17})$$

The counterparts to the first two constraints in the computational basis (Eqs. (B5) and (B6)) are trivial. This is because the distance [48] between supporting states (equivalent to Δ_i in the computational stage) in Eq. (B15) is 1.

This constraint again reduces the possible set of errors, yielding the density matrix

$$\rho_2 = \sum_{\bar{x} \in \mathcal{E}_2} p(\bar{x}) |\tilde{\varphi}_{\bar{x}}\rangle \langle \tilde{\varphi}_{\bar{x}}| , \quad (\text{B18})$$

$$\mathcal{E}_2 = \left\{ \bar{x} = (s_A, s_B, l_A, l_B) \in \mathcal{E} : \begin{array}{l} s_A = A_1 \pmod{\Delta_i} \\ s_B = B_1 \pmod{\Delta_i} \\ s_A - s_B = A_1 - B_1 \pmod{\Delta_c} \\ l_A + l_B = -(A_2 + B_2) \pmod{m_c/m_f} \end{array} \right\} , \quad (\text{B19})$$

with the state after the second measurement being

$$|\tilde{\varphi}_{\bar{x}}\rangle = \sum_{k=0}^{m_f-1} \left| (\Delta_f k + A_2)_+^{m_c} \right\rangle_A \left| (-\Delta_f k + B_2 + \Delta_f v)_+^{m_c} \right\rangle_B , \quad (\text{B20})$$

where $\Delta_f = \frac{m_c}{m_f}$ and $\Delta_f v = -(l_A + l_B + A_2 + B_2)$.

Alice applies a rotation in the dual basis by $-A_2$, which corresponds to the addition or removal of photons. Bob calculates the best possible dual-basis rotation, chosen to maximize the likelihood of successful realignment (similarly to the first stage):

$$v_B = \arg \max_{v \in \{0, \dots, m_f-1\}} \left(\sum_{\substack{t=0, \pm 1, \dots, \pm m_c-1 \\ j=0, \pm 1, \dots, \pm (\Delta_c-1)}} P_{l=-A_2+t} \cdot P_{l=-B_2-t-v \frac{m_c}{m_f} + j \cdot m_c} \right) . \quad (\text{B21})$$

Bob rotates his cavity in the dual basis by $-v_B \Delta_f - B_2$, resulting in the state

$$\sum_{k=0}^{m_f-1} \left| (\Delta_f k)_+^{m_c} \right\rangle_A \left| (-\Delta_f k + \Delta_f (v - v_B))_+^{m_c} \right\rangle_B. \quad (\text{B22})$$

This equation shows that a successful realignment is achieved when

$$v = v_B \pmod{m_c}. \quad (\text{B23})$$

To calculate the fidelity of this distilled state to the desired target state, we can sum over the probabilities for all errors that result in a successful realignment, i.e., for which Eqs. $u_B = -u$, and $v_B = v$ are satisfied. This set is given by

$$\mathcal{S} = \left\{ \bar{x} = (s_A, s_B, l_A, l_B) \in \mathcal{E} : \begin{array}{l} s_A = A_1 \pmod{\Delta_i} \\ s_B = B_1 \pmod{\Delta_i} \\ s_A - s_B = A_1 - B_1 + u_B \Delta_c \pmod{d} \\ l_A + l_B = -(A_2 + B_2) + v_B \Delta_f \pmod{d} \end{array} \right\}. \quad (\text{B24})$$

For specific measurement outcomes (A_1, B_1, A_2, B_2) , the fidelity to the target state is the ratio between the total probability of error configurations \bar{x} that lead to a successful realignment and the total probability of the set \mathcal{E}_2 of all error configurations \bar{x} capable of yielding these particular outcomes. This can be expressed as

$$\mathcal{F}_{A_1, B_1, A_2, B_2} = \sum_{\bar{x} \in \mathcal{S}} p(\bar{x}) / \sum_{\bar{x} \in \mathcal{E}_2} p(\bar{x}). \quad (\text{B25})$$

The fidelity of the distillation protocol \mathcal{F}_{avg} is obtained by averaging over all possible measurement outcomes, i.e.,

$$\mathcal{F}_{\text{avg}} = \sum_{A_1, B_1, A_2, B_2} \mathcal{F}_{A_1, B_1, A_2, B_2} \cdot p_{A_1, B_1, A_2, B_2}. \quad (\text{B26})$$

Here, p_{A_1, B_1, A_2, B_2} is the probability of a specific measurement outcome. Since each error \bar{x} has $\frac{m_i}{m_c}$ different outcomes for the angular measurements and $\frac{m_c}{m_f}$ for the photon number measurements, we obtain the following identity:

$$p_{A_1, B_1, A_2, B_2} = \frac{m_f}{m_i} \sum_{\bar{x} \in \mathcal{E}_2} p(\bar{x}). \quad (\text{B27})$$

If the protocol abort step is included, i.e., $f_{\text{cut}} > 0$, we restrict our attention to only those measurement outcomes for which the fidelity exceeds f_{cut} . In this case, the average fidelity is computed using only those outcomes A_1, B_1, A_2, B_2 that satisfy $\mathcal{F}_{A_1, B_1, A_2, B_2} > f_{\text{cut}}$:

$$\mathcal{F}_{\text{avg}} = \sum_{\substack{A_1, B_1, A_2, B_2 \\ \text{s.t. } \mathcal{F}_{A_1, B_1, A_2, B_2} > f_{\text{cut}}}} \mathcal{F}_{A_1, B_1, A_2, B_2} \cdot p_{A_1, B_1, A_2, B_2}. \quad (\text{B28})$$

This also introduces a failure probability, p_{abort} , expressed as

$$p_{\text{abort}} = \sum_{\substack{A_1, B_1, A_2, B_2 \\ \text{s.t. } \mathcal{F}_{A_1, B_1, A_2, B_2} \leq f_{\text{cut}}}} p_{A_1, B_1, A_2, B_2}. \quad (\text{B29})$$

Appendix C: No-communication protocol

In Figure 5 of the main text, we compare the performance of the distillation protocol with a strategy in which there is no communication between the parties. In this section, we describe the no-communication protocol in more detail. After completing a modular measurement in either the computational or dual basis, each party independently

applies a phase-space rotation to their respective cavity based solely on their own measurement outcomes (A_1, A_2 and B_1, B_2 for Alice and Bob, respectively).

There are $\Delta_c(\Delta_f)$ possible measurement outcomes and $m_c(m_f)$ different rotations for aligning the state with $|0\rangle$ ($|0_+\rangle$). A map between the outcomes and rotations can be described by a function for each of the two protocol stages, namely $f_O : \mathbb{Z}_{\Delta_c} \rightarrow \mathbb{Z}_{m_c}$ and $g_O : \mathbb{Z}_{\Delta_f} \rightarrow \mathbb{Z}_{m_f}$ with $O \in \{A, B\}$.

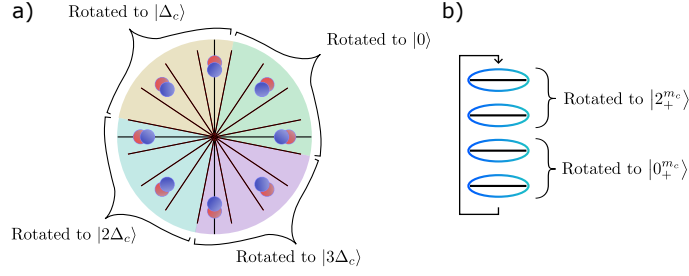


FIG. 10. Illustration of a no-communication strategy, represented in phase space (a) and in modular Fock space (b). In this case, $d = 16$, $m_i = 8$, and $m_c = 4$. The blue and red circles represent the states of Alice and Bob prior to the modular phase measurements. After the angular measurement of $O_1 \in \{0, \dots, \Delta_c - 1\}$, one optimal strategy is to rotate the resulting state clockwise by $-O_1$. In other words, the rotation function is $f(O_1) = 0$, meaning we always rotate to the closest alignment clockwise. The dual basis rotation function is $g(O_2) = 0$, meaning we always rotate to the closest aligned state with fewer photons. The no-communication strategy can be thought of as a coarse-graining of the cavity phase space. For example, in the computational basis, measurement outcomes ranging from $\lfloor 1 - \Delta_i/2 \rfloor$ to $\lfloor \Delta_c - \frac{1}{2}\Delta_i \rfloor$ are all merged to the same state.

These functions describe the rotation each party performs as follows:

$$\begin{aligned} X^{-O_1 + \Delta_c f_O(O_1)}, \\ Z^{-O_2 + \Delta_f g_O(O_2)}. \end{aligned}$$

These rotations ensure that the state is realigned with $|0\rangle$ and $|0_+^{m_c}\rangle$, respectively. This realignment can be written by applying the rotations to the measured state from Eq. (B8) after the rotations:

$$\begin{aligned} X_A^{-A_1 + \Delta_c f_A(A_1)} X_B^{-B_1 + \Delta_c f_B(B_1)} |\tilde{\varphi}_{\bar{x}}\rangle = \\ \frac{1}{\sqrt{m_c}} \sum_{k'=0}^{m_c-1} c_{k'} |\Delta_c(k' + f_A(A_1))\rangle_A |\Delta_c(k' + u + f_B(B_1))\rangle_B, \end{aligned} \quad (C1)$$

and similarly using Eq. (B20) for the dual basis.

The maps f_X , g_X are chosen to maximize the probability for a successful alignment between the cavities, i.e. to maximize the fidelity to the state $\frac{1}{\sqrt{m_c}} \sum_{k'} c_{k'} |\Delta_c k'\rangle_A |\Delta_c k'\rangle_B$.

Due to the symmetry between the two parties, we assume $f_A = f_B$ and $g_A = g_B$.

We focus first on the dephasing correction stage. Since we assume that large misalignments in the computational basis (i.e., $u > 1$) are highly unlikely, the optimal strategy for $f(O)$ is binary: $f(O_1) = 0$ corresponds to a clockwise rotation to the nearest aligned configuration, while $f(O_1) = 1$ indicates a counter-clockwise rotation to the closest aligned state.

Before addressing the general scenario, consider a case where the separation between supporting sections of the initial state is two, i.e., $\Delta_i = d/m_i = 2$ (see Fig. 10). In this case, an even measurement outcome O_1 is most likely associated with no dephasing error. Odd results of O_1 are most likely the result of a dephasing rotation by one section. However, the outcome does not convey information on the direction of the dephasing error. Therefore, the optimal strategy is to choose a constant function for

f , whose value represents a predetermined decision on whether to align the state with $|0\rangle$ or with $|\Delta_c\rangle$.

In the general scenario with $\Delta_i > 2$, the measurement outcome can convey information on the direction of the errors. That is, the measurement has a sufficiently high resolution to indicate whether the dephasing error was likely a clockwise or a counterclockwise rotation.

In this case, it can be shown that the optimal function f changes its value in the middle between two supporting states, i.e. $\lceil (n + \frac{1}{2})\Delta_i \rceil$ for any $n \in \mathbb{Z}_{m_i/m_c}$. This function can be written as

$$f_n(O_1) = \begin{cases} 0 & O_1 \leq \lceil (n + \frac{1}{2})\Delta_i \rceil \\ 1 & O_1 > \lceil (n + \frac{1}{2})\Delta_i \rceil \end{cases}. \quad (C2)$$

Note that the specific choice of n is arbitrary due to the translation symmetry of the initial state.

Following Appendix B, the criterion for a successful realignment is

$$s_A - s_B = A_1 - B_1 + u_{NC}\Delta_c \pmod{d}, \quad (C3)$$

with $u_{NC} = (f(A_1) - f(B_1))$.

For the loss correction stage, the result O_2 does not convey any information on the underlying noise, since all dual-basis states participate equally in the intermediate cavity state. Thus, there is no preferred direction for rotation, and we set $g(O_2) = 0$.

Appendix D: Distilling higher-entanglement states ($m_f > 2$)

For certain cases, distilled states with higher entanglement entropy may be desirable. In our protocol, this corresponds to setting $m_f > 2$. In this section, we evaluate the performance of the protocol for $m_f = 4$, which corresponds to an entanglement entropy of $E_f = 2$ for the target state.

Increasing m_f while keeping d and m_i constant reduces the separation between states in either the dephasing

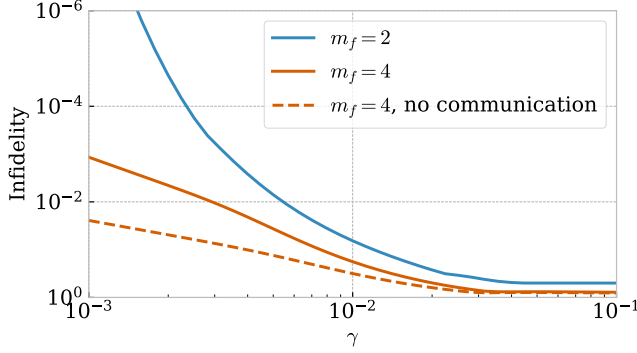


FIG. 11. Average protocol infidelity as a function of noise coefficients ($\gamma_l = \gamma_\phi = \gamma$) for $m_f = 2$ and $m_f = 4$. $d = m_i = 16$, and m_c is independently optimized for each noise coefficient value.

correction stage or the loss correction stage. The balance between the performance of these two stages is determined by m_c , which is now also confined to a smaller set of values, $m_f \leq m_c \leq m_i$.

Figure 11 compares the performance of the protocol for $m_f = 2$ and $m_f = 4$, with the optimal m_c selected for each case. Although a higher m_f compromises the protocol performance, a high distillation fidelity is still achieved compared to the no-communication protocol.

Appendix E: Distillation of initial states with low entanglement entropy

When analyzing the distillation protocol, it is not evident that choosing an initial state with higher entanglement entropy than that of the desired target state results in a higher fidelity of the distilled state.

To illustrate this, consider the 4-level qudit case with dephasing noise \mathcal{N}_D as described in Section II D. Alice can directly prepare the target state $|\psi'_i\rangle = |\psi_t\rangle = \frac{1}{\sqrt{2}}(|00\rangle + |22\rangle)$ instead of the proposed initial state $|\psi_i\rangle =$

$\frac{1}{\sqrt{4}}(|00\rangle + |11\rangle + |22\rangle + |33\rangle)$. The initial state $|\psi'_i\rangle$ has an entanglement entropy of $E(|\psi'_i\rangle) = 1$, whereas the proposed state has $E(|\psi_i\rangle) = 2$. The state goes through the noise channel, and its fidelity degrades. When applying the protocol to the noisy state $\mathcal{N}_D(|\psi'\rangle\langle\psi'|)$, the same fidelity is obtained as for the case of the proposed state $|\psi_i\rangle$.

However, this property is not unique to our distillation protocol. In traditional qubit-based distillation protocols, one can also identify initial states with low entanglement entropy yielding identical distillation performance to the typical highly-entangled initial state consisting of multiple Bell pairs. For example, we consider the recurrence distillation protocol [8] applied to two noisy Bell pairs, i.e., two e-bits, described by the state $W_F \otimes W_F$. Here, W_F is the Werner state

$$W_F = \Delta_F(|\Psi^-\rangle\langle\Psi^-|) = F|\Psi^-\rangle\langle\Psi^-| + \frac{1-F}{3}(|\Psi^+\rangle\langle\Psi^+| + |\Phi^-\rangle\langle\Phi^-| + |\Phi^+\rangle\langle\Phi^+|), \quad (\text{E1})$$

where Δ_F is the depolarizing channel with parameter F acting on one qubit of the Bell pair, and $\{|\Psi^\pm\rangle, |\Phi^\pm\rangle\}$ are the Bell basis states. Alternatively, the protocol could be applied to the 1-ebit state $(\Delta_F \otimes \Delta_F)(|00\rangle_A|11\rangle_B + |11\rangle_A|00\rangle_B)$ and obtain the same target state with identical fidelity. This fact demonstrates that a higher initial entanglement entropy does not necessarily translate into a distilled state with higher fidelity. However, the initial state with low entanglement entropy is harder to produce, and so starting with multiple Bell pairs is preferable.

The same principle applies to our bosonic entanglement distillation protocol. As described in Section III A, the state $|\psi_i\rangle$ is easier to produce than $|\psi'_i\rangle$, as it requires shorter gate times. Moreover, when both loss and dephasing errors are present, preparing the relevant state with low entanglement entropy requires a complex initialization procedure [21], making its preparation even more challenging.

Appendix F: Bosonic operations

In this section, we elaborate on the bosonic continuous-variable operations described in section III.

1. Phase measurements

Canonical phase measurements are described by the set of POVM's $\{M(\theta)\}$ where θ is the measured phase [21, 33]. The elements of this set can be represented as:

$$M(\theta) = \frac{1}{2\pi} \sum_{m,n=0}^{\infty} e^{i(m-n)\theta} |m\rangle\langle n|. \quad (\text{F1})$$

Since we are interested in measuring whether the phase is in a particular section defined by the interval $\theta \in$

$\left(\frac{(2k-1)\pi}{d}, \frac{(2k+1)\pi}{d}\right)$, we integrate over the phase and obtain the section measurement POVM element

$$M_k = \int_{\frac{(2k-1)\pi}{d}}^{\frac{(2k+1)\pi}{d}} M(\theta) d\theta = \frac{1}{2\pi} \sum_{m,n=0}^{\infty} \Gamma_{n,m}^k |m\rangle \langle n|, \quad (\text{F2})$$

with

$$\Gamma_{n,m}^k = \begin{cases} \frac{1}{i(m-n)} (e^{i(m-n)(2k+1)\pi/d} - e^{i(m-n)(2k-1)\pi/d}) & m \neq n \\ \frac{2\pi}{d} & m = n \end{cases}. \quad (\text{F3})$$

2. Primitive states

The two primitive states we use in this work are the coherent and the squeezed-coherent states.

The coherent state $|\alpha\rangle$ is defined by acting with the displacement operator on the cavity vacuum state $|0\rangle$, i.e.,

$$|\alpha\rangle = \mathcal{D}(\alpha) |0\rangle \equiv e^{\alpha \hat{a}^\dagger - \alpha^* \hat{a}} |0\rangle. \quad (\text{F4})$$

To reduce the overlap between primitive states in adjacent sections, squeezed coherent states $|\alpha, \zeta\rangle = \mathcal{D}(\alpha) \mathcal{S}(\zeta) |0\rangle$ can be used instead, where the squeezing operator $\mathcal{S}(\zeta)$ with squeezing parameter ζ is defined as

$$\mathcal{S}(\zeta) \equiv e^{\frac{1}{2}(\zeta \hat{a}^{\dagger 2} - \zeta^* \hat{a}^2)}. \quad (\text{F5})$$

3. Initial state preparation

In this section, we describe the preparation of the initial entangled state for the distillation protocol. The basic building block is the controlled rotation gate CROT^{1/m_i} defined as

$$\text{CROT}^{1/m_i} := e^{i \frac{2\pi}{m_i} \hat{n}_A \hat{n}_B}.$$

The action of the CROT^{1/m_i} gate can be understood by considering its effect on a pair of cavities: one initialized in an arbitrary state $|\psi\rangle_A$ and the other in a Fock state $|j\rangle_B$. Specifically, the CROT_{AB}^{1/m_i} gate performs a rotation on the first cavity by an angle $2\pi j/m_i$, denoted by $R_{2\pi j/m_i}^A$, i.e.,

$$\text{CROT}_{AB}^{1/m_i} |\psi\rangle_A |j\rangle_B = R_{2\pi j/m_i}^A |\psi\rangle_A |j\rangle_B. \quad (\text{F6})$$

The preparation procedure consists of a channel \mathcal{C}_x acting on the two cavities A, B and an ancilla cavity C , each prepared in the primitive state $|0^{\text{CV}}\rangle = |\Theta\rangle$. This channel, illustrated in Fig. 7, consists of a CROT_{AC}^{1/m_i} gate between the first cavity and the ancilla and another CROT_{BC}^{1/m_i} gate between the second cavity and the ancilla, followed by a Z -basis measurement on the ancilla cavity.

The application of the two entangling gates results in

$$\text{CROT}_{AC}^{1/m_i} \text{CROT}_{BC}^{1/m_i} (|0^{\text{CV}}\rangle_A |0^{\text{CV}}\rangle_B |0^{\text{CV}}\rangle_C) = \text{CROT}_{AC}^{1/m_i} \text{CROT}_{BC}^{1/m_i} \left(|0^{\text{CV}}\rangle_A |0^{\text{CV}}\rangle_B \sum_{k=0}^{m_i-1} \frac{1}{\sqrt{m_i}} |k_+^{\text{CV}}\rangle_C \right) \quad (\text{F7})$$

$$= \frac{1}{\sqrt{m_i}} \sum_{k=0}^{m_i-1} |k^{\text{CV}}\rangle_A |k^{\text{CV}}\rangle_B |k_+^{\text{CV}}\rangle_C \quad (\text{F8})$$

$$= \frac{1}{\sqrt{m_i}} \sum_{k=0}^{m_i-1} |k^{\text{CV}}\rangle_A |k^{\text{CV}}\rangle_B \sum_j e^{-2ijk\pi/m_i} |j^{\text{CV}}\rangle_C. \quad (\text{F9})$$

Here, we defined the dual basis states as $|k_+^{\text{CV}}\rangle = \frac{1}{\sqrt{\mathcal{N}_k}} \sum_{j=0}^{d-1} e^{-2ijk\pi/d} |j^{\text{CV}}\rangle$, where the normalization coefficient $\sqrt{\mathcal{N}_k} = d$ is constant under the approximation that rotated primitive states $|k^{\text{CV}}\rangle \equiv R_{2k\pi/d} |\Theta\rangle$ are mutually orthogonal,

i.e., $\langle 0^{\text{CV}} | k^{\text{CV}} \rangle = 0$ for every $k \in \mathbb{Z}_d$. Each state in this basis is supported only by photon numbers $|n\rangle$ satisfying $n = k \pmod{d}$, leading to the second equality in (F8). We also assumed $m_i = d$.

Finally, when measuring the ancilla cavity in the logical Z -basis, and obtaining the result x , we obtain the desired initial state

$$\mathcal{C}_x(|0^{\text{CV}}\rangle_A |0^{\text{CV}}\rangle_B |0^{\text{CV}}\rangle_E) = \frac{1}{\sqrt{m_i}} \sum_{k=0}^{m_i-1} e^{-2ikx\pi/m} |k^{\text{CV}}\rangle_A |k^{\text{CV}}\rangle_B \quad (\text{F10})$$

up to a phase that can be tracked in software.

Appendix G: Decoding the continuous-variable distilled state

To evaluate the fidelity of our final state in the continuous-variable description, we apply a decoding map $\mathcal{D} \otimes \mathcal{D}$ to a two-qudit Hilbert space of dimension d^2 .

Here, we opt to implement the decoding process by utilizing the angular-section definition of the d -dimensional qudit. We do so by using the Pegg-Barnett states [49]

$$|\phi, s\rangle \equiv \frac{1}{\sqrt{s}} \sum_{n=0}^{s-1} e^{in\phi} |n\rangle . \quad (\text{G1})$$

which provide an orthonormal basis $\{|\phi = 2\pi m/s, s\rangle\}_{m=0, \dots, s-1}$ for the truncated s -dimensional Fock space. When $s \rightarrow \infty$, the basis states become confined to a particular phase ϕ in the bosonic phase space. Since we want our map to be dependent on the angular section, yet indifferent to the angular degree of freedom within the section, we use this basis to trace out the angular degree of freedom inside each section.

For our purposes, we adopt an alternative representation of the Pegg-Barnett states $|i, \phi\rangle$, associating them with a particular angular section i and angle ϕ relative to the section's center. This is expressed by

$$|i, \phi = 2\pi m/s\rangle \equiv |\phi = 2\pi(i/d + m/s), s\rangle \quad (\text{G2})$$

with $i \in \mathbb{Z}_d$ and $m \in \{-s/2d, \dots, s/2d - 1\}$.

To extract a logical qudit from a continuous variable mixed state ρ (which we assume can be truncated due to its finite energy), the decoding map \mathcal{D} traces out the degrees of freedom inside the angular section ϕ . The matrix elements of the resulting d -dimensional qudit density matrix σ are given by

$$\sigma_{ij} = \mathcal{D}(\rho)_{ij} = \sum_{m=-s/2d}^{s/2d-1} \langle i, \phi = 2\pi m/s | \rho | j, \phi = 2\pi m/s \rangle . \quad (\text{G3})$$

with $i, j \in \mathbb{Z}_d$.

For a system of two cavities, A and B , with density matrix ρ_{AB} , we extend the trace-out procedure in a similar way. The elements of the reduced density matrix σ in the d^2 -dimensional two-qudit space are defined by

$$\sigma_{i_A, i_B, j_A, j_B} = \sum_{m=-s/2d}^{s/2d-1} \sum_{l=-s/2d}^{s/2d-1} \langle i_A, \phi = 2\pi m/s |_A \langle i_B, \phi = 2\pi l/s |_B \rho_{AB} |j_A, \phi = 2\pi m/s\rangle_A |j_B, \phi = 2\pi l/s\rangle_B , \quad (\text{G4})$$

with $i_A, i_B, j_A, j_B \in \mathbb{Z}_d$.

Using this reduced density matrix, we evaluate the logical fidelity of the distilled bosonic state with respect to a desired discrete target state $|\psi_t\rangle$ (see Fig. 8). The fidelity conditioned on a specific set of measurement outcomes (A_1, B_1, A_2, B_2) is given by

$$\mathcal{F}(A_1, B_1, A_2, B_2) = F(\sigma(A_1, B_1, A_2, B_2), |\psi_t\rangle \langle \psi_t|) . \quad (\text{G5})$$

- A. Peres, and W. K. Wootters, Teleporting an unknown quantum state via dual classical and einstein-podolsky-rosen channels, *Phys. Rev. Lett.* **70**, 1895 (1993).
- [3] L. Jiang, J. M. Taylor, K. Nemoto, W. J. Munro, R. Van Meter, and M. D. Lukin, Quantum repeater with encoding, *Phys. Rev. A* **79**, 032325 (2009).
- [4] A. K. Ekert, Quantum cryptography based on bell's theorem, *Phys. Rev. Lett.* **67**, 661 (1991).
- [5] A. K. Ekert and R. Renner, The ultimate physical limits of privacy, *Nature* **507**, 443 (2014).
- [6] J. I. Cirac, A. K. Ekert, S. F. Huelga, and C. Macchiavello, Distributed quantum computation over noisy channels, *Phys. Rev. A* **59**, 4249 (1999).
- [7] N. H. Nickerson, Y. Li, and S. C. Benjamin, Topological quantum computing with a very noisy network and local error rates approaching one percent, *Nature communications* **4**, 1756 (2013).
- [8] C. H. Bennett, G. Brassard, S. Popescu, B. Schumacher, J. A. Smolin, and W. K. Wootters, Purification of noisy entanglement and faithful teleportation via noisy channels, *Physical Review Letters* **76**, 722–725 (1996).
- [9] C. H. Bennett, D. P. DiVincenzo, J. A. Smolin, and W. K. Wootters, Mixed-state entanglement and quantum error correction, *Physical Review A* **54**, 3824–3851 (1996).
- [10] D. Deutsch, A. Ekert, R. Jozsa, C. Macchiavello, S. Popescu, and A. Sanpera, Quantum privacy amplification and the security of quantum cryptography over noisy channels, *Physical Review Letters* **77**, 2818–2821 (1996).
- [11] W. Dür, H.-J. Briegel, J. I. Cirac, and P. Zoller, Quantum repeaters based on entanglement purification, *Physical Review A* **59**, 169–181 (1999).
- [12] R. Matsumoto, Conversion of a general quantum stabilizer code to an entanglement distillation protocol, *Journal of Physics A: Mathematical and General* **36**, 8113–8127 (2003).
- [13] N. Kalb, A. A. Reiserer, P. C. Humphreys, J. J. W. Bakermans, S. J. Kamerling, N. H. Nickerson, S. C. Benjamin, D. J. Twitchen, M. Markham, and R. Hanson, Entanglement distillation between solid-state quantum network nodes, *Science* **356**, 928–932 (2017).
- [14] R. Reichle, D. Leibfried, E. Knill, J. Britton, R. B. Blakestad, J. D. Jost, C. Langer, R. Ozeri, S. Seidelin, and D. J. Wineland, Experimental purification of two-atom entanglement, *Nature* **443**, 838 (2006).
- [15] M. Zwerger, A. Pirker, V. Dunjko, H. Briegel, and W. Dür, Long-range big quantum-data transmission, *Physical Review Letters* **120** (2018).
- [16] T. A. Hahn, R. White, H. Bernien, and R. Arnon-Friedman, *Deterministic high-rate entanglement distillation with neutral atom arrays* (2025), [arXiv:2503.00445 \[quant-ph\]](https://arxiv.org/abs/2503.00445).
- [17] D. Gottesman, A. Kitaev, and J. Preskill, Encoding a qubit in an oscillator, *Physical Review A* **64** (2001).
- [18] P. T. Cochrane, G. J. Milburn, and W. J. Munro, Macroscopically distinct quantum-superposition states as a bosonic code for amplitude damping, *Physical Review A* **59**, 2631–2634 (1999).
- [19] M. H. Michael, M. Silveri, R. T. Brierley, V. V. Albert, J. Salmilehto, L. Jiang, and S. M. Girvin, New class of quantum error-correcting codes for a bosonic mode, *Phys. Rev. X* **6**, 031006 (2016).
- [20] V. V. Albert, K. Noh, K. Duivenvoorden, D. J. Young, R. T. Brierley, P. Reinhold, C. Vuillot, L. Li, C. Shen, S. M. Girvin, B. M. Terhal, and L. Jiang, Performance and structure of single-mode bosonic codes, *Physical Review A* **97** (2018).
- [21] A. L. Grimsmo, J. Combes, and B. Q. Baragiola, Quantum computing with rotation-symmetric bosonic codes, *Physical Review X* **10** (2020).
- [22] C. Flühmann, T. L. Nguyen, M. Marinelli, V. Negnevitsky, K. Mehta, and J. Home, Encoding a qubit in a trapped-ion mechanical oscillator, *Nature* **566**, 513 (2019).
- [23] M. Mirrahimi, Z. Leghtas, V. V. Albert, S. Touzard, R. J. Schoelkopf, L. Jiang, and M. H. Devoret, Dynamically protected cat-qubits: a new paradigm for universal quantum computation, *New Journal of Physics* **16**, 045014 (2014).
- [24] L. Hu, Y. Ma, W. Cai, X. Mu, Y. Xu, W. Wang, Y. Wu, H. Wang, Y. P. Song, C.-L. Zou, S. M. Girvin, L.-M. Duan, and L. Sun, Quantum error correction and universal gate set operation on a binomial bosonic logical qubit, *Nature Physics* **15**, 503–508 (2019).
- [25] N. Ofek, A. Petrenko, R. Heeres, P. Reinhold, Z. Leghtas, B. Vlastakis, Y. Liu, L. Frunzio, S. M. Girvin, L. Jiang, *et al.*, Extending the lifetime of a quantum bit with error correction in superconducting circuits, *Nature* **536**, 441 (2016).
- [26] V. V. Sivak, A. Eickbusch, B. Royer, S. Singh, I. Tsioutsios, S. Ganjam, A. Miano, B. L. Brock, A. Z. Ding, L. Frunzio, S. M. Girvin, R. J. Schoelkopf, and M. H. Devoret, Real-time quantum error correction beyond break-even, *Nature* **616**, 50–55 (2023).
- [27] P. Campagne-Ibarcq, A. Eickbusch, S. Touzard, E. Zalts-Geller, N. E. Frattini, V. V. Sivak, P. Reinhold, S. Puri, S. Shankar, R. J. Schoelkopf, L. Frunzio, M. Mirrahimi, and M. H. Devoret, Quantum error correction of a qubit encoded in grid states of an oscillator, *Nature* **584**, 368–372 (2020).
- [28] Z. Ni, S. Li, X. Deng, Y. Cai, L. Zhang, W. Wang, Z.-B. Yang, H. Yu, F. Yan, S. Liu, *et al.*, Beating the break-even point with a discrete-variable-encoded logical qubit, *Nature* **616**, 56 (2023).
- [29] D. Lachance-Quirion, M.-A. Lemonde, J. O. Simoneau, L. St-Jean, P. Lemieux, S. Turcotte, W. Wright, A. Lacroix, J. Fréchette-Viens, R. Shillito, F. Hopfmueller, M. Tremblay, N. E. Frattini, J. Camirand Lemyre, and P. St-Jean, Autonomous quantum error correction of Gottesman-Kitaev-Preskill states, *Phys. Rev. Lett.* **132**, 150607 (2024).
- [30] J. Eisert, S. Scheel, and M. B. Plenio, Distilling gaussian states with gaussian operations is impossible, *Physical Review Letters* **89** (2002).
- [31] R. Namiki, O. Gittsovich, S. Guha, and N. Lütkenhaus, Gaussian-only regenerative stations cannot act as quantum repeaters, *Physical Review A* **90** (2014).
- [32] P. Leviant, Q. Xu, L. Jiang, and S. Rosenblum, Quantum capacity and codes for the bosonic loss-dephasing channel, *Quantum* **6**, 821 (2022).
- [33] A. S. Holevo, *Probabilistic and statistical aspects of quantum theory* (Springer Science & Business Media, 2011) Chap. 4.
- [34] A. Grimm, N. E. Frattini, S. Puri, S. O. Mundhada, S. Touzard, M. Mirrahimi, S. M. Girvin, S. Shankar, and M. H. Devoret, Stabilization and operation of a Kerr-cat qubit, *Nature* **584**, 205 (2020).
- [35] L. Sun, A. Petrenko, Z. Leghtas, B. Vlastakis, G. Kirchmair, K. M. Sliwa, A. Narla, M. Hatridge, S. Shankar,

- J. Blumoff, L. Frunzio, M. Mirrahimi, M. H. Devoret, and R. J. Schoelkopf, Tracking photon jumps with repeated quantum non-demolition parity measurements, *Nature* **511**, 444 (2014).
- [36] C. S. Wang, J. C. Curtis, B. J. Lester, Y. Zhang, Y. Y. Gao, J. Freeze, V. S. Batista, P. H. Vaccaro, I. L. Chuang, L. Frunzio, *et al.*, Efficient multiphoton sampling of molecular vibronic spectra on a superconducting bosonic processor, *Physical Review X* **10**, 021060 (2020).
- [37] J. M. Gertler, B. Baker, J. Li, S. Shirol, J. Koch, and C. Wang, Protecting a bosonic qubit with autonomous quantum error correction, *Nature* **590**, 243 (2021).
- [38] L. Jiang, J. M. Taylor, A. S. Sørensen, and M. D. Lukin, Distributed quantum computation based on small quantum registers, *Physical Review A—Atomic, Molecular, and Optical Physics* **76**, 062323 (2007).
- [39] I. Rojko, M. Simoni, E. Zapusek, F. Reiter, and J. Home, Stabilization of cat-state manifolds using nonlinear reservoir engineering, (2024), [arXiv:2407.18087](#).
- [40] S. Konno, W. Asavanant, F. Hanamura, H. Nagayoshi, K. Fukui, A. Sakaguchi, R. Ide, F. China, M. Yabuno, S. Miki, H. Terai, K. Takase, M. Endo, P. Marek, R. Filip, P. van Loock, and A. Furusawa, Logical states for fault-tolerant quantum computation with propagating light, *Science* **383**, 289–293 (2024).
- [41] O. Milul, B. Guttel, U. Goldblatt, S. Hazanov, L. M. Joshi, D. Chausovsky, N. Kahn, E. Çiftyürek, F. Lafont, and S. Rosenblum, Superconducting cavity qubit with tens of milliseconds single-photon coherence time, *PRX Quantum* **4**, 030336 (2023).
- [42] P. Magnard, S. Storz, P. Kurpiers, J. Schär, F. Marxer, J. Lütolf, T. Walter, J.-C. Besse, M. Gabureac, K. Reuer, A. Akin, B. Royer, A. Blais, and A. Wallraff, Microwave quantum link between superconducting circuits housed in spatially separated cryogenic systems, *Phys. Rev. Lett.* **125**, 260502 (2020).
- [43] C. J. Axline, L. D. Burkhardt, W. Pfaff, M. Zhang, K. Chou, P. Campagne-Ibarcq, P. Reinhold, L. Frunzio, S. M. Girvin, L. Jiang, M. H. Devoret, and R. J. Schoelkopf, On-demand quantum state transfer and entanglement between remote microwave cavity memories, *Nature Physics* **14**, 705 (2018).
- [44] L. D. Burkhardt, J. D. Teoh, Y. Zhang, C. J. Axline, L. Frunzio, M. Devoret, L. Jiang, S. Girvin, and R. Schoelkopf, Error-detected state transfer and entanglement in a superconducting quantum network, *PRX Quantum* **2**, 030321 (2021).
- [45] A. Almanakly, B. Yankelevich, M. Hays, B. Kannan, R. Assouly, A. Greene, M. Gingras, B. M. Niedzielski, H. Stickler, M. E. Schwartz, K. Serniak, J. I.-J. Wang, T. P. Orlando, S. Gustavsson, J. A. Grover, and W. D. Oliver, [Deterministic remote entanglement using a chiral quantum interconnect](#) (2024), [arXiv:2408.05164](#).
- [46] S. Storz, J. Schär, A. Kulikov, P. Magnard, P. Kurpiers, J. Lütolf, T. Walter, A. Copetudo, K. Reuer, A. Akin, *et al.*, Loophole-free bell inequality violation with superconducting circuits, *Nature* **617**, 265 (2023).
- [47] S. Bravyi, M. Suchara, and A. Vargo, Efficient algorithms for maximum likelihood decoding in the surface code, *Physical Review A* **90** (2014).
- [48] Here, “distance” refers to the minimum number of errors required to transform one supporting state into another.
- [49] S. Barnett and D. Pegg, On the hermitian optical phase operator, *Journal of Modern Optics* **36**, 7 (1989).